Fault propagation and climatic control of sedimentation on the Ghoubbet Rift Floor: insights from the Tadjouraden cruise in the western Gulf of Aden

L Audin, I Manighetti, P Tapponnier, F Métivier, E Jacques, Philippe Huchon

Geophys. J. Int. (2001) **144,** 391–413

Fault propagation and climatic control of sedimentation on the Ghoubbet Rift Floor: insights from the Tadjouraden cruise in the western Gulf of Aden

L. Audin,[1] I. Manighetti,[1] P. Tapponnier,[1] F. Métivier,[1] E. Jacques[1] and P. Huchon[2]

[1] *IPGP, Laboratoire de Tectonique,* 4 *place Jussieu,* 75005 *Paris, France. E-mail: audin@ipgp.jussieu.fr*
[2] *ENS, Laboratoire de Geologie,* 24 *rue Lhomond,* 75005 *Paris, France*

Accepted 2000 September 5. Received 2000 September 5; in original form 1999 April 13

SUMMARY

A detailed geophysical survey of the Ghoubbet Al Kharab (Djibouti) clarifies the small-scale morphology of the last submerged rift segment of the propagating Aden ridge before it enters the Afar depression. The bathymetry reveals a system of antithetic normal faults striking N130°E, roughly aligned with those active along the Asal rift. The 3.5 kHz sub-bottom profiler shows how the faults cut distinct layers within the recent, up to 60 m thick, sediment cover on the floor of the basin. A large volcanic structure, in the centre of the basin, the 'Ghoubbet' volcano, separates two sedimentary flats. The organization of volcanism and the planform of faulting, with *en echelon* subrifts along the entire Asal–Ghoubbet rift, appear to confirm the westward propagation of this segment of the plate boundary. Faults throughout the rift have been active continuously for the last 8400 yr, but certain sediment layers show different offsets. The varying offsets of these layers, dated from cores previously retrieved in the southern basin, imply Holocene vertical slip rates of 0.3–1.4 mm yr^{-1} and indicate a major decrease in sedimentation rate after about 6000 yr BP. The two central sub-basins E and W of the volcano have distinct depositional histories and the Ghoubbet may have been isolated from the sea between 10 and 72 kyr BP.

Key words: climatic control, fault propagation, Gulf of Aden, sedimentation.

1 INTRODUCTION

The nearly land-locked sea gulf of the Ghoubbet Al Kharab lies along the westernmost rift segment of the Arabia–Somalia plate boundary (e.g. Manighetti *et al.* 1997). Between 25 Ma and the present, the Sheba ridge appears to have propagated westwards from the Alula Fartak fracture zone (Fig. 1) to the Afar depression (Courtillot *et al.* 1980, 1984; Cochran 1981; Manighetti *et al.* 1997; 1998). The segment at the tip of the propagating ridge, the Asal–Ghoubbet rift, is unique because its emerged western half exposes in unrivalled detail the tectonic processes that precede the onset of seafloor spreading. Such exceptional exposure, between the Ghoubbet Gulf and Lake Asal (Figs 1 and 2), has fostered in-depth studies of that part of the rift (Tazieff *et al.* 1972; Stieltjes 1973, 1980; Varet & Gasse 1978; Ruegg *et al.* 1979, 1984, 1990; Ruegg & Kasser 1987; Abdallah *et al.* 1979; Le Dain *et al.* 1979; Demange *et al.* 1980; Stein *et al.* 1991; De Chabalier & Avouac 1994; Manighetti *et al.* 1998). The Asal–Ghoubbet rift (Fig. 2) exhibits most of the characteristic features of slow-spreading-ridge axial segments (Barberi *et al.* 1972; Tapponnier & Varet 1974), in particular a narrow trough, ~10 km wide and 40 km long, bounded by normal faults (Stieltjes 1980) showing fast Holocene vertical throw rates (1–4 mm yr^{-1}, Stein *et al.* 1991), and a volcanic zone with contemporaneous volcanic and tectonic activity (1978 seismic sequence, Ruegg *et al.* 1980; Abdallah *et al.* 1979; Le Dain *et al.* 1979). Extension occurs in a mean N40°E direction at a rate of ~17 mm yr^{-1} (De Chabalier & Avouac 1994; Stein *et al.* 1991; Manighetti *et al.* 1998). Seismic refraction profiles show a thinning of seismic layers and anomalous low-velocity mantle under the Asal–Ghoubbet rift (Ruegg 1974), as found beneath active oceanic ridges. The localization of faulting in the emerged Asal–Ghoubbet area is characterized by subrifts (Dankalelo and Disa Le Mallo subrifts, Fig. 2) with north-westward-younging tectonic and volcanic ages and a recent jump from the southern to the northern subrift (Manighetti *et al.* 1998). This subrift diachronicity has been interpreted to reflect the northwestwards propagation of the Arabia–Somalia plate boundary into Afar (Manighetti *et al.* 1997) on a local scale.

Previous data in the Ghoubbet Gulf has been insufficient to determine fault geometry or map volcanic edifices and to locate the faults responsible for the deformation recorded by

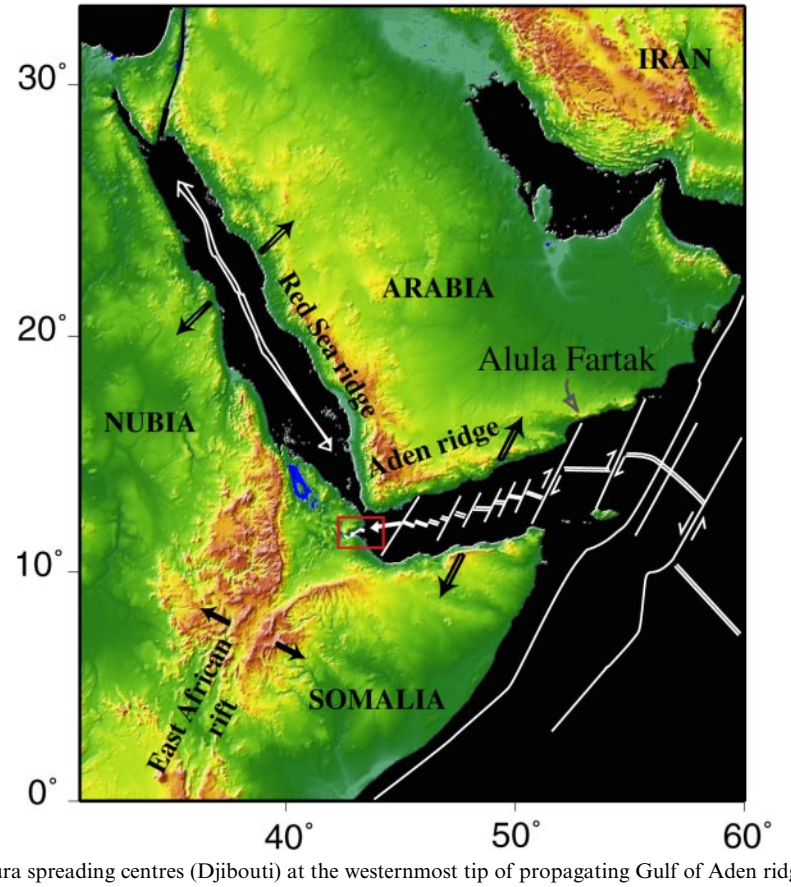

Figure 1. Location of Tadjoura spreading centres (Djibouti) at the westernmost tip of propagating Gulf of Aden ridge. Red rectangle indicates the location of the Asal–Ghoubbet rift.

the geodetic and seismological networks, particularly those activated during the 1978 volcanotectonic sequence, the largest earthquake of which ($mb = 5.3$) occurred underwater (Le Dain *et al.* 1979; Ruegg *et al.* 1980). Although extant bathymetric profiles (Bäcker *et al.* 1973) suggest the presence of steep slopes due to active faulting, submersible observations from three dives in the Ghoubbet (Fig. 2a, Choukroune *et al.* 1986) showed no trace of shallow faulting cutting sea-bottom sediments (Choukroune *et al.* 1988). Several questions thus remain unanswered. What is the overall geometry of the Asal–Ghoubbet rift? Is it possible to quantify underwater deformation on individual faults and to constrain the rift kinematics? How is seismicity in the Ghoubbet related to faults cutting its floor? Is there evidence of propagation in the submarine part of the rift, as observed on land? In order to elucidate such problems, new geophysical data (Figs 2 and 3a) were acquired during the Tadjouraden cruise in the summer of 1995. The corresponding multibeam bathymetry (Figs 2 and 3a), coupled with acoustic imagery and 3.5 kHz sub-bottom profiler sections, now yields a much improved view of the geometry of faults, volcanic edifices and sedimentary deeps in the Ghoubbet basin, and hence of the overall structure and tectonics of the Asal–Ghoubbet rift.

2 DATA SETS

In August–September 1995, the French R/V Atalante cruised the western Gulf of Aden from ~46°E to the western tip of the Ghoubbet basin at 42°30′E (Fig. 2). 20 profiles with simultaneous use of EM12/950 echosounders, sub-bottom profiler (3.5 kHz) and side-scan sonar were obtained in the Ghoubbet basin (Fig. 2a). GPS navigation allowed ship positioning within ±50 m accuracy and enabled near-shore work. The close spacing of the profiles provided complete multibeam bathymetry and imagery of the basin (Figs 2, 3 and 4). The vertical and lateral resolutions of the bathymetric data were ±0.5–1.0 m and ±5 m, respectively (Fig. 2). The resulting bathymetric map was combined with the digital elevation model of the emerged part of the rift between Ghoubbet and Asal (De Chabalier & Avouac 1994; vertical and lateral resolutions of ±1 m and ±15 m, respectively) to produce an accurate topographic image of the whole rift (Figs 2 and 3a). Perturbations of bathymetric and topographic gradients were used to detect and map major faults and volcanic structures. Slope steepening between linear slope breaks was used to define major fault scarps and to estimate surface fault throw. Volcanic edifices were mapped from the roughly concentric closely spaced depth contours surrounding them (Fig. 2). Artificial lighting was used to enhance tectonic and volcanic features (Fig. 3a). The Ghoubbet being fairly shallow (maximum depth ~220 m), sedimentary and volcanic surfaces were separated on the basis of their backscatter level or echo 'intensity' on the multibeam acoustic imagery, which is related to seafloor 'hardness' (Augustin *et al.* 1996; Fig. 4). These backscatter images also outline major fault scarps, in the form of dark (or bright) narrow and continuous lines (Fig. 4).

The 3.5 kHz sub-bottom profiler penetrated up to 60 m into the soft sediments covering the Ghoubbet floor, making a succession of distinct layers visible (Fig. 4b). The profiles were

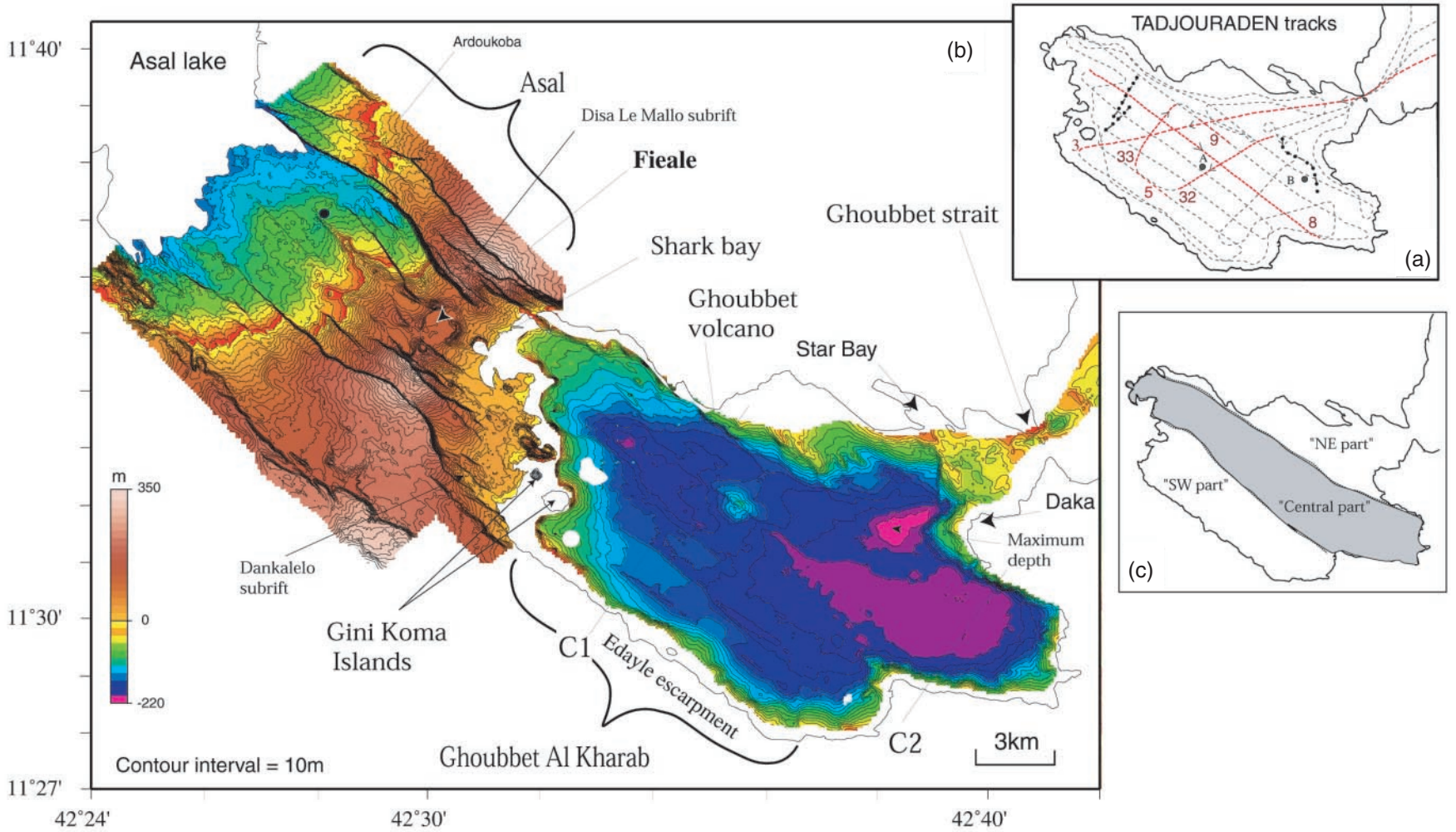

Figure 2. (a) Tadjouraden ship tracks in Ghoubbet basin (dashed lines). Red dashed lines are 3.5 kHz profiles: P3, P33, P8, P32 shown in Figs 5, 9, 10 and 11, respectively. Dots A and B are Orgon IV cores drilled in 1981 (CEPM-CNEXO 1981), with four dated samples. Dash-dotted lines represent CYADEN dive tracks (Choukroune *et al.* 1986). (b) Merged bathymetric and topographic map of the Asal–Ghoubbet rift zone from subaerial DEM topography (De Chabalier & Avouac 1994) and from the bathymetric survey of the Tadjouraden cruise. Locations of cross-sections C1 and C2 (Fig. 3) are indicated. (c) Definition of the three main parts of the Ghoubbet basin.

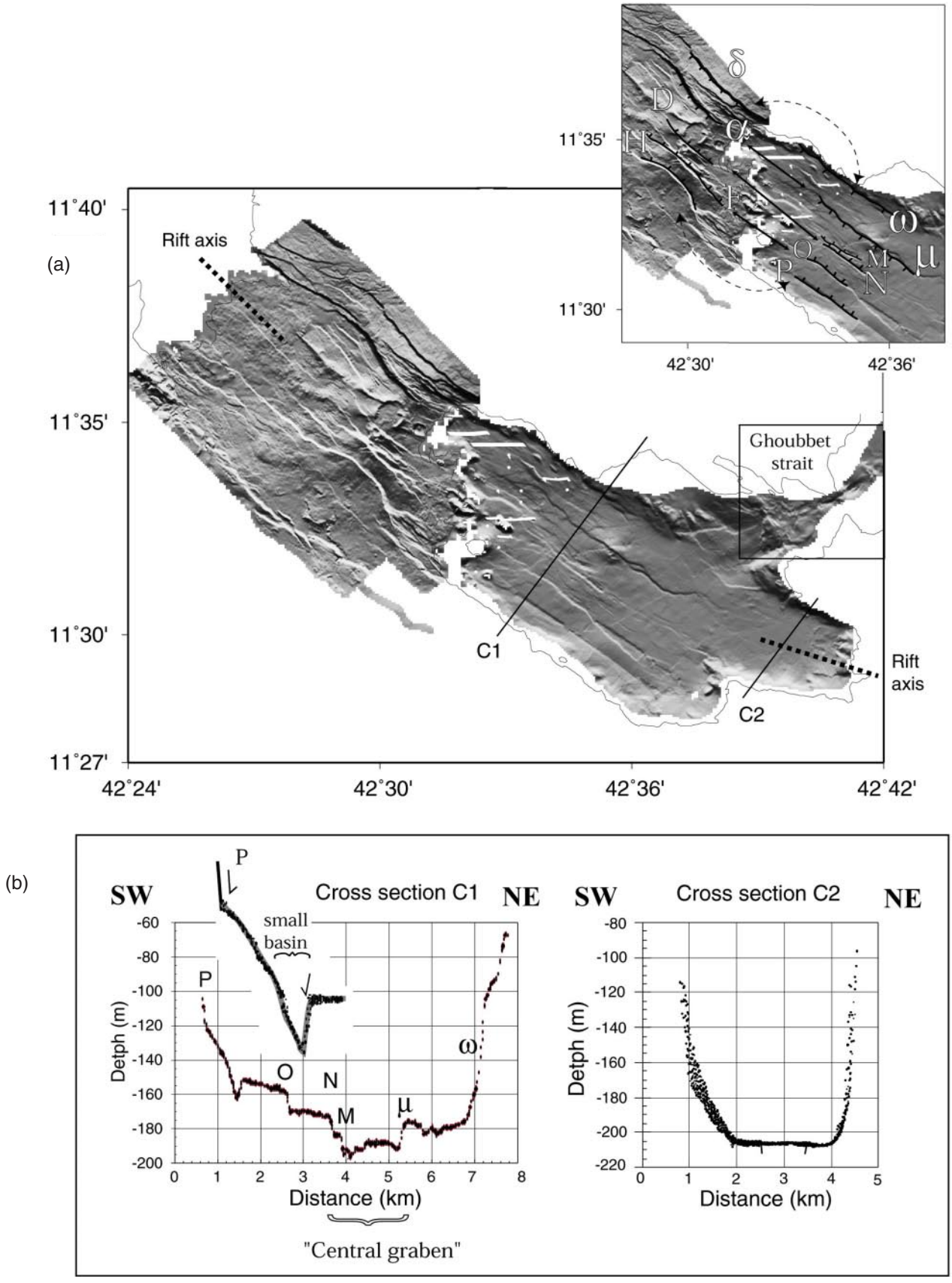

Figure 3. (a) Shaded relief of the Asal–Ghoubbet rift segment (040° illumination; merged DEM + Tadjouraden bathymetry). Dashed bold lines indicate rift axis. Inset shows major faults on land and underwater, with corresponding letter symbols. Curved dashed arrows point to the equivalence of outer boundary faults. (b) Bathymetric sections C1 and C2 (location in Fig. 2) across Ghoubbet trough showing rift-in-rift and simpler structure in the west and east, respectively. Both profiles run perpendicular to the N130°E trend of Ghoubbet.

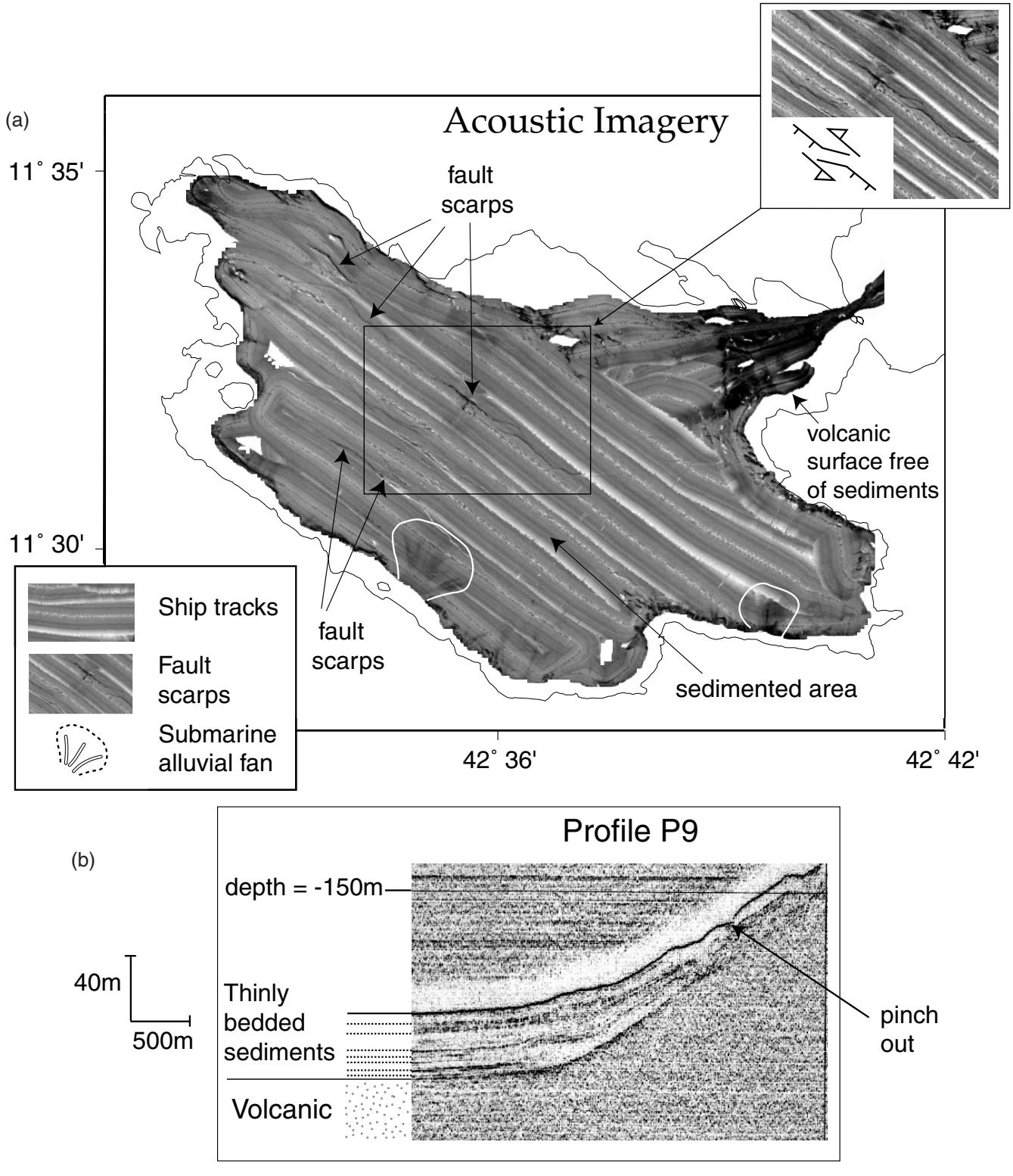

Figure 4. (a) Acoustic imagery from the Tadjouraden survey with examples of submarine fans, fault scarps and different reflective surfaces (volcanics or sediments). (b) The 3.5 kHz sub-bottom profile P9 (see profile location of Fig. 2a) shows thin laminations within sediment cover that differ from more homogeneous and massive rocks interpreted as volcanic basement.

depth-corrected assuming a compressional *P*-wave velocity of 1500 m s^{-1} (that of seawater) for the sediments. Assuming that the porosity of the sediments is high, that is, the sediments are full of water, makes such a correction reasonable. The resulting precision of depth measurements is ± 1 m. The seafloor offsets on the profiles help one to detect, follow and map faults in greater detail than would be possible just from the bathymetry and seafloor imagery alone (Fig. 5). Identification and

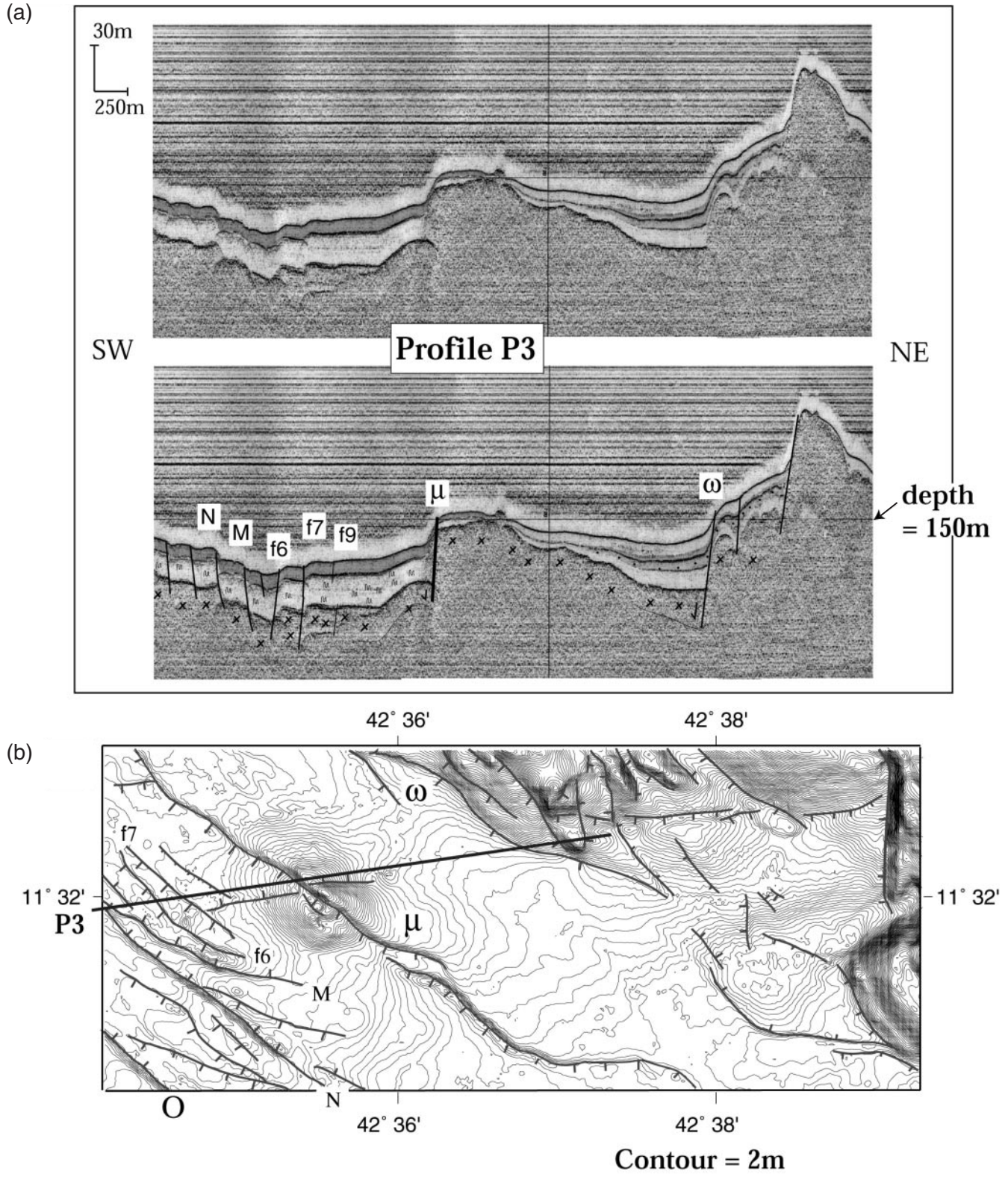

Figure 5. (a) Interpretation of faulted sedimentary cover on 3.5 kHz profile P3 (see profile location in Fig. 2a). P3 crosses the axial rift and the north slope of Ghoubbet volcano. Grey layers represent individual sediment layers on either side of the volcano (NE and SW sub-basins). Fault symbols and locations as in Fig. 6. Fault locations are coherent with fault traces identified on the bathymetric map of Fig. 5(b). (b) Corresponding bathymetric map (contour interval = 2 m) with fault traces in planform and their respective names. P3 is shown as a bold line.

correlation of different sedimentary layers or volcanic surfaces on the foot-and hangingwalls of faults yielded estimates of their throws and of the variation of throw along strike and with depth. The combination of our measurements with previous stratigraphic and chronological data (Gasse & Richard 1981) was used to infer slip rates on certain major faults.

Finally, our data and observations were integrated with onshore data, in particular fault mapping based on satellite and aerial images (e.g. Manighetti *et al.* 1998), to produce a synthetic volcanotectonic map of the Asal–Ghoubbet rift. Our results show that active normal faulting and volcanism are as prominent beneath the Ghoubbet Gulf as they are along the emerged rift stretching between Asal and the Ghoubbet, making the actual 'Asal–Ghoubbet' rift up to 40 km long.

3 DATA ANALYSIS

3.1 Overall morphology of the Ghoubbet basin

The Ghoubbet basin is a NW–SE-trending, ~25 km long, ~10 km wide trough in line with the ~N130°E Asal rift (Fig. 2a). Its floor, bounded by steep parallel NE–NNE to SW–SSW-facing scarps, is 180–200 m deep on average, with a tendency to deepen eastwards. At a more detailed level, the floor depth and morphology vary significantly both along and across strike (Figs 2–4). The Ghoubbet can be divided into three main parallel NW-striking parts (Fig. 2c). The central part is a long (~25 km) and narrow (4–5 km) axial deep, limited by steep cumulative scarps, that are particularly clear where they meet the gulf's eastern coast (Figs 2–6). The overall strike of this axial graben curves slightly counterclockwise from ~N130°E in the NW to near E–W in the east, where it notches the coast. A large central volcano, ~2 km across, has grown in the middle of the graben floor, dividing it into two distinct NW and SE basins. The southern basin is larger (~5.5 km), on average deeper (~210 m) than the northern one (~3.6 km, ~190 m), and has a broader, flatter, less faulted floor.

The SW part of the Ghoubbet basin is an uplifted ledge, shorter (~15 km long) and shallower (~120–140 m) than the axial graben. This ledge, which extends all the way to the steep Edayle coastal escarpment, is dissected in a series of faulted benches, parallel to the southern coast, that step down towards the axial deep (Figs 2–6). A few narrow (~500 m) finger-shaped channels disrupt the continuity of these benches. The southeasternmost bench is covered by three large submarine fans fed by the deep canyons that incise the Edayle escarpment (Fig. 6).

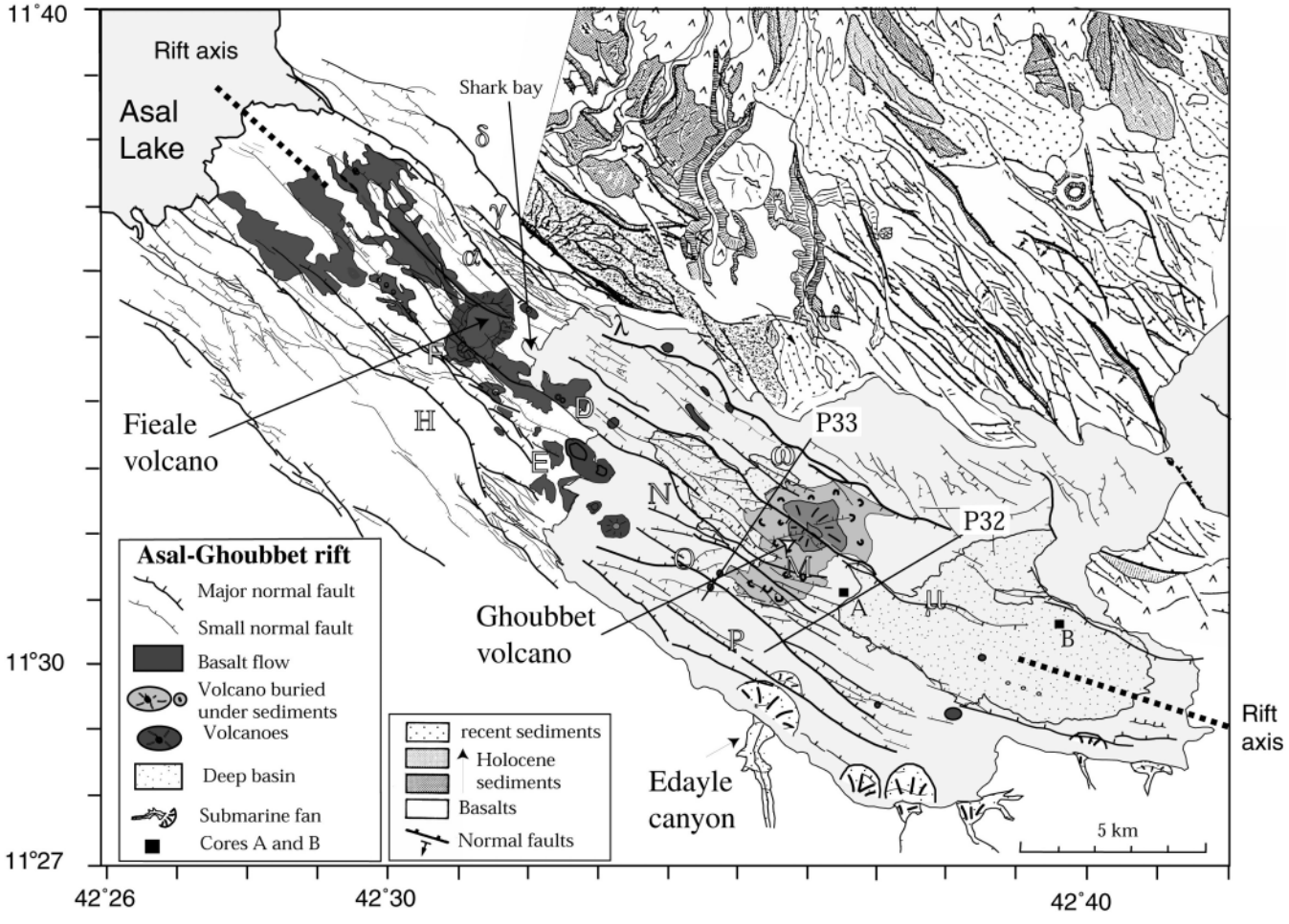

Figure 6. Overall structural interpretation of the Asal–Ghoubbet rift based on combined bathymetry, acoustic imagery and 3.5 kHz profiler data. Fault trace thickness reflects offset size. Onshore faulting is from Manighetti *et al.* (1998).

The NE part is a complexly faulted shelf, on average less than 100 m deep, between the axial graben and the northern Ghoubbet coast, which extends all the way to the shallow Ghoubbet Strait. This shelf is dissected by NNW- to N-striking scarps, at high angles to the axial rift faults, in line with the scarps that structure and disrupt the northern coast (Fig. 6). Such oblique faults may be related to bookshelf faulting, documented on land by Manighetti *et al*. (1998). The emerged normal fault network north of the Ghoubbet Strait (Fig. 6), for instance, appears to be rotated clockwise as it accommodates the transfer of extension between the overlapping Tadjoura and Asal–Ghoubbet rifts (Tapponnier *et al*. 1990; Manighetti *et al*. 1998). A particularly deep (>220 m) basin that strikes ENE, oblique to the axial rift, cuts the southeastern part of the shelf, mostly north of the northern main bounding scarp of the rift. The NE shelf shallows towards the Ghoubbet Strait, which is 25 m deep at its shallowest.

The shaded image of Fig. 3(a) brings out the linearity and continuity of the major scarps that control the bathymetry of the central part of the basin, showing their morphological similarity to those of the active normal faults of the Asal rift. The bathymetric profile across the northwestern part of the Ghoubbet (Fig. 3b) shows the steepness of these scarps, the innermost of which face each other to bound the inner floor of the central graben, as at Asal (e.g. Manighetti *et al*. 1998). It is thus clear that the overall morphology of the Ghoubbet basin results from normal faulting, which is described below in detail.

3.2 Fault geometry

The main normal faults in the Ghoubbet (P, O, M+N, μ, ω; Figs 3 and 6) appear to be the southeastward equivalent of the faults that control the topography of the Asal rift (H, F, D, α, δ). The average strike of the longest and highest cumulative scarps along these faults, however, is ~N125°E, hence slightly more easterly than the ~N130°E strike of the Asal rift faults (Fig. 7). Like the Asal faults, the longest Ghoubbet faults are up to 10 km long and their cumulative scarps are up to ~100 m high. They connect with smaller normal faults, striking on average either N100±5°E or N145±5°E (Figs 6 and 7). The overall fault distribution is not uniform. Faults appear to be more closely spaced in the northwestern half of the Ghoubbet, whereas the smooth southeastern graben floor is hardly faulted at all (Figs 5a, 6 and 8). There is also clear asymmetry. Normal faults dipping to the NE are predominant (Figs 3a and 7), as in the Asal rift (e.g. Stein *et al*. 1991). In particular, the 'SW ledge' is chiefly defined by NE-dipping faults, the largest of which (P, O, M+N, length ~9 km and throw >20 m) appear to be arranged in a right-stepping fashion. At the southeast extremities of faults N and O (Fig. 5), smaller, more easterly striking normal faults have formed. Some of them, antithetic to faults N and O, isolate narrow, wedge-shaped grabens (length ~1–4.5 km, width ~250–500 m, depth >5–10 m). Such narrow grabens taper westwards with a sharp tip, a feature identified and interpreted as evidence of propagation in the Asal rift (Manighetti *et al*. 1998).

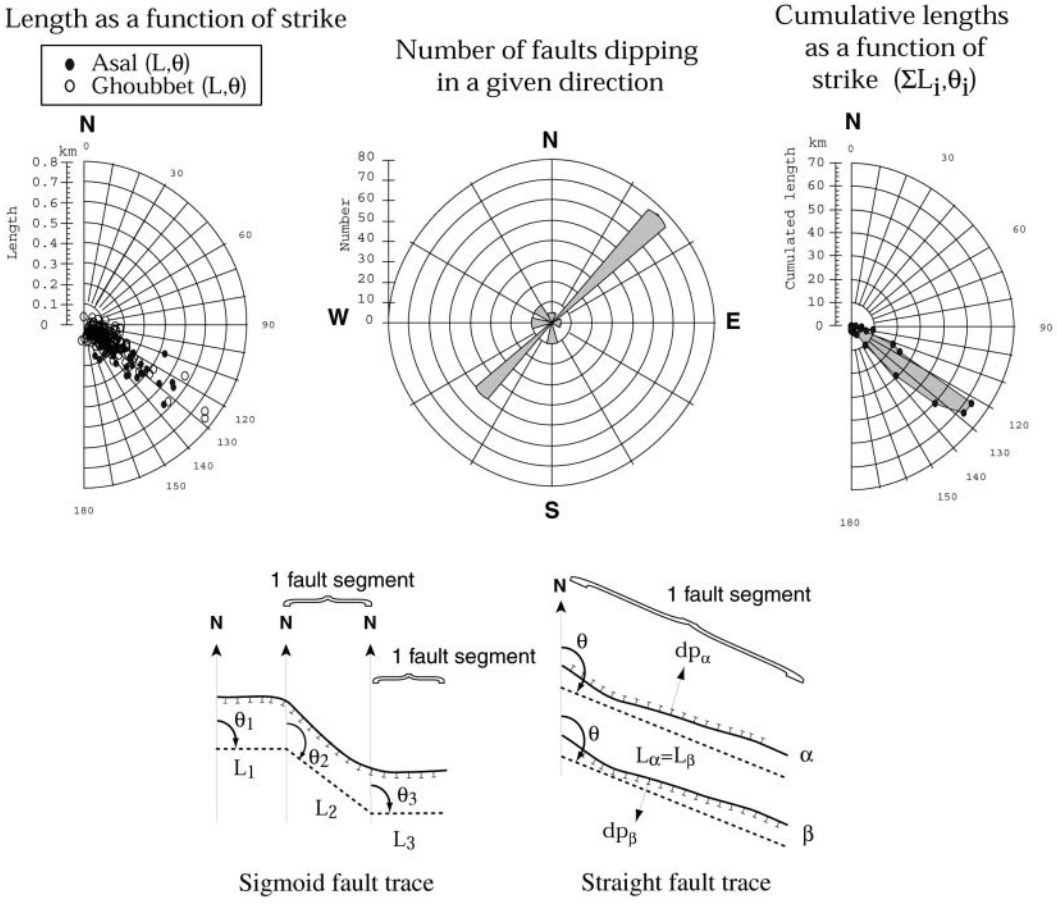

Figure 7. Polar plots of lengths, number of faults with a given dip direction and cumulative lengths as a function of orientation in the Asal–Ghoubbet rift. Sketch illustration of strategy used for measuring length (L), strike (θ) and dip direction (dp) and for defining individual fault segments.

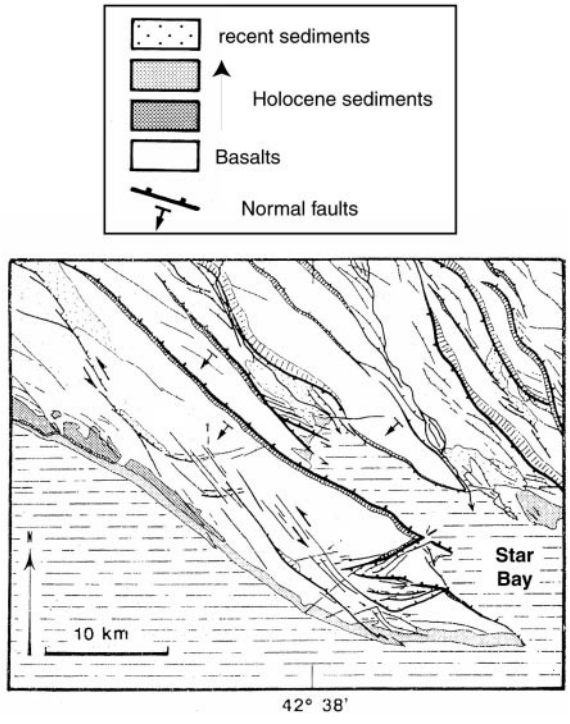

Figure 8. Faulting near Star bay area from a SPOT image interpretation (Manighetti 1993).

The central graben inner floor is bounded to the north by a more continuous, though sinuous, SW-dipping normal fault (μ), about 12 km long, with a throw of at least 20 m, that cuts through the summit crater of the central Ghoubbet volcano (Fig. 5). The axial graben width narrows from 3.8 to 1.3 km from east to west, so that this graben also tapers westwards with a sharp tip encroaching onshore (Figs 2 and 6).

Towards the east, the northern boundary fault μ curves counterclockwise, while its throw decreases markedly (Fig. 5). The inner graben floor thus widens to merge progressively with the undisturbed floor of the easternmost Ghoubbet (Figs 2, 3b and 6). As a result of the right-stepping geometry of its southern boundary faults, the central graben inner floor, and hence the rift axis, progressively shifts northwards as one goes from SE to NW. North of its westward tip, only one major south-dipping fault scarp (λ) can be identified, continuing onshore across the coastline to merge with fault γ. In both the SW and central parts of the Ghoubbet rift, most of the main ~N120°E-striking faults exhibit either linear traces splaying into or connected with more easterly secondary normal faults (e.g. O and μ) or sigmoid kinks (e.g. μ, Figs 5 and 6). Both the first (horsetail) and second (extensional jog) geometries are indicative of a left-lateral component of slip, as documented on land (Manighetti *et al.* 1998).

The NE shelf of the Ghoubbet is cut by a series of parallel N150±20°E-striking normal faults, with ~2 km long, 20–100 m high scarps, most of which face southwestwards. To the east, such faults seem to be associated with secondary ~EW-striking faults, as seen on land (e.g. near Star Bay, Figs 6 and 8). Some of the N150°E-striking faults probably correspond to those observed on land across the coast in an area characterized by parallel tilted basaltic strips (Manighetti 1993; Figs 6 and 8).

3.3 Volcanism

The combined bathymetry, imagery and 3.5 kHz profiles permit identification of volcanic structures and products, whether exposed on the seafloor or hidden below the sediment cover (Figs 9 and 10). Like that of the Asal rift further west, most of the recent Ghoubbet basement appears to be made of basaltic lavas (e.g. Fig. 10). We could identify several volcanic edifices on the Ghoubbet rift floor, mostly in its western half (Fig. 6). Several volcanoes, some of them hyaloclastite vents (e.g. Gini Koma Islands; Fig. 2) lie between the Asal rift coastline and the western tip of the Ghoubbet basin. Together with Fieale Koma, the main central volcano of the Asal rift (Fig. 6; Stieltjes 1980), they form a line of mature volcanic structures. The large central volcanic edifice that interrupts the axial Ghoubbet graben has a roughly circular shape, and is smaller than Fieale (Figs 6 and 10b). Its conical relief protrudes from the sediment cover, suggesting that most of the effusives that built it were emplaced before sediment deposition. Most of the lava flows that we infer from our data to have originated from this 'Ghoubbet volcano' appear to be overlain by the sediment cover (Fig. 10). Small lateral volcanic vents, probably related to the Ghoubbet volcano, are also clear south of it, along fault N. They are now hidden by the sediment cover (Fig. 10). Other small volcanic vents are aligned along faults ω, μ, M in the northwestern part of the basin, close to the coast, some of them protruding above the sediment cover (Figs 2 and 6).

3.4 Sediment nature and distribution

The multibeam sonar imagery shows that much of the floors of the two Ghoubbet sub-basins are covered with sediments. Large submarine fans are visible only along the base of the southern Edayle boundary escarpment, facing the SE sub-basin (Figs 2, 4 and 6). On the 3.5 kHz profiles, the sediment cover forms a layer about 45 m thick on average, composed of distinct layers (Figs 5 and 9–11). The profiles show that the number and thicknesses of these layers are variable. This is particularly clear along the eight NW-trending profiles (Fig. 2b) that cross the Ghoubbet rift along strike (e.g. P8 on Fig. 10).

In the NW basin, between the northwestern coast and the Ghoubbet volcano, two distinct sedimentary horizons (pink and yellow, Fig. 10b) 10 and 20 m thick, the bottom one perhaps subdivided into two layers, overlie a layer that appears to be made of more massive rock, with rougher surfaces and no internal layering, that tapers at the foot of the volcano. Hence, we interpret this basal layer to be composed of basalts (Fig. 4b). The thicknesses of the sedimentary layers decrease progressively up the flanks of the volcano but exhibit sudden changes across the rift faults (Figs 9 and 10).

In the deeper southeastern basin, between the volcano and the eastern coast of the Ghoubbet, five distinct, clearly stratified sedimentary horizons, with thicknesses ranging between ~4 and 12 m, are visible (Figs 10 and 11). This difference suggest that the Ghoubbet volcano isolated the western from the eastern basin, and probably from marine sedimentation, in recent history.

Two cores, drilled over 15 years ago into the Ghoubbet floor (A, B, Figs 2b and 6; IGN 1953 Tadjoura geological map; Gasse & Richard 1981), show stratified muds overlain by a thin layer (<0.5 m) of detrital material (Fig. 11b and c and Fig. 12). Both cores were retrieved in the southwestern sub-basin. In

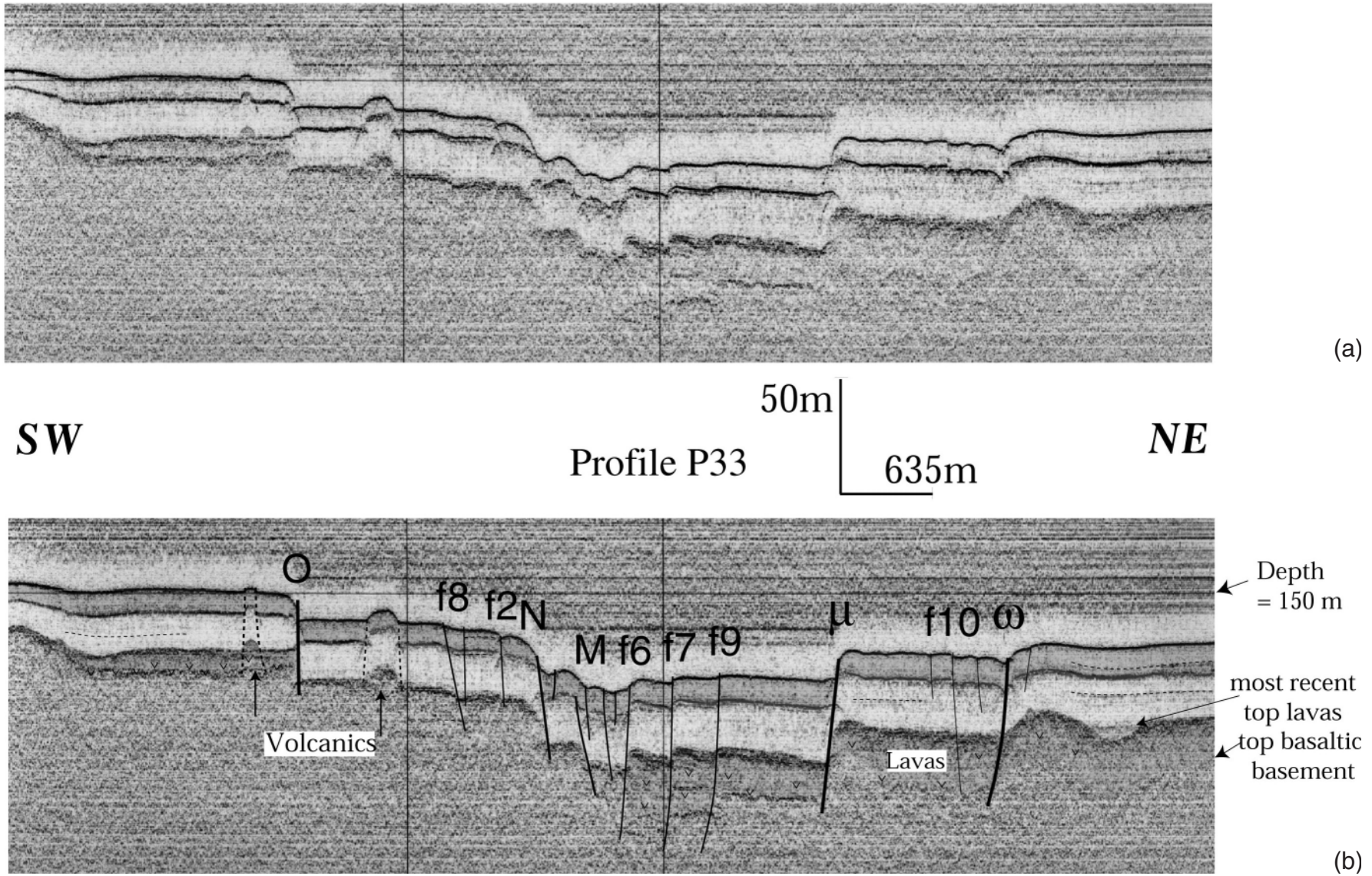

Figure 9. 3.5 kHz profile P33 (see location in Fig. 2a) across the axial rift structure. Grey layers represent individual sediment layers in the NW basin. Fault names (symbols) and locations are from Fig. 6. Fault locations are coherent with fault traces identified in the bathymetric map of Fig. 2.

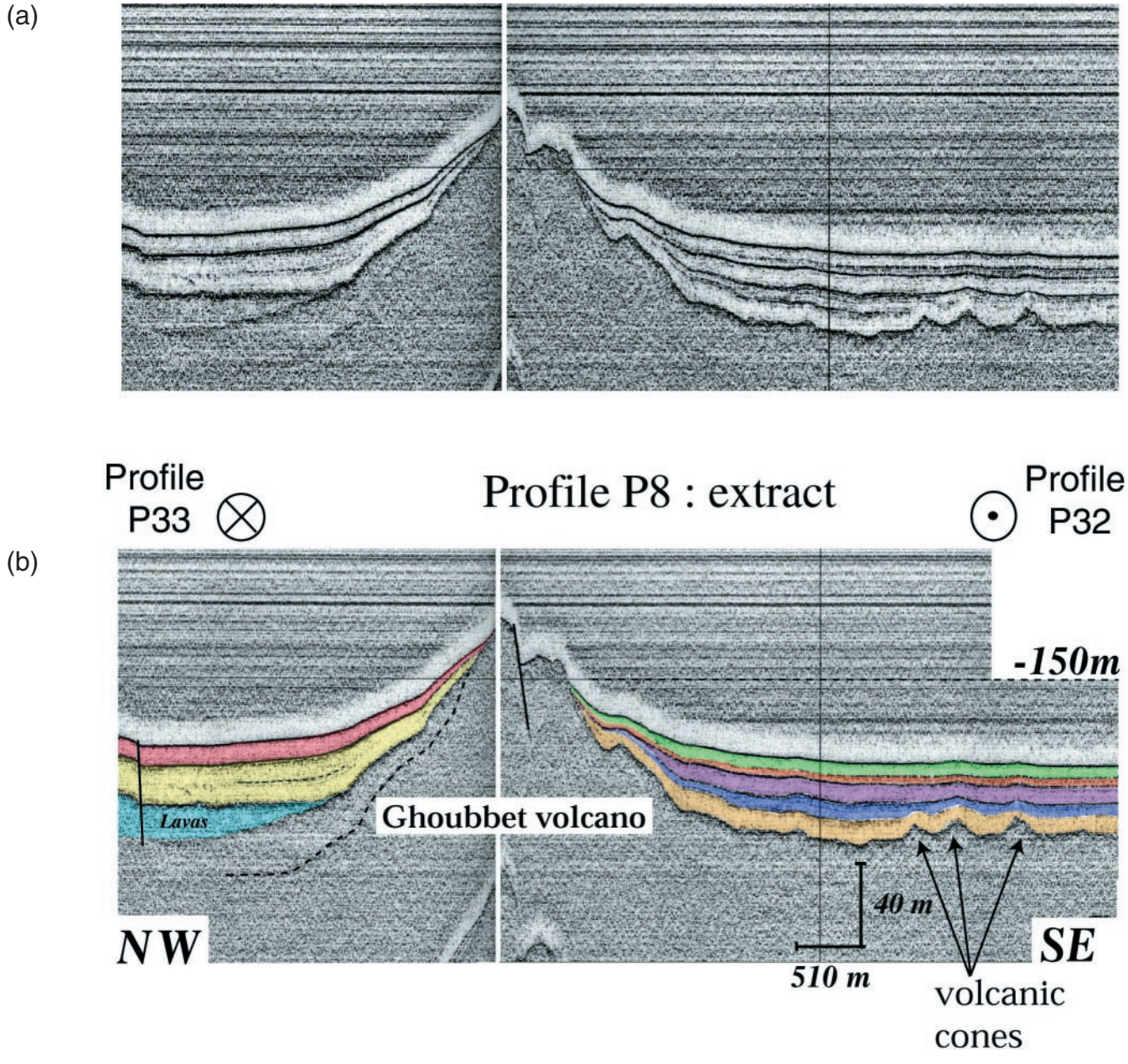

Figure 10. 3.5 kHz profile P8 (see location in Fig. 2a), roughly along the μ normal fault and the across Ghoubbet volcano. Colours represent individual sediment layers on either side of the volcano. Fault names and locations are from Fig. 6. Fault locations are coherent with fault traces identified in the bathymetric map of Fig. 2.

both, a level of fine-grained volcanic glass and ashes was identified within a thin, dark horizon at a depth of ~5 m. Each core shows marine sedimentation with either diatomitic deposits (8–6 kyr BP; 4–15 m) or detrital sediments (6–0 kyr BP; 0–4 m; Gasse & Richard 1981). Core A, ~11 m long, was drilled close to profile P32 (Figs 2b and 6). Comparison of the thicknesses and interface depths of the layers identified on P32 and in core A implies that they reflect the same stratigraphic sequence. We plotted each dated sample on the 3.5 kHz log (Figs 11c and 12) to illustrate the correlation between the two data sets. Table 1 summarizes the ages of layer 1 (1730 to 5950 a), layer 2 (7760 a) and layer 3 (8400 a). Our data imply that these layers, all of them of Holocene age, drape the entire southwestern sub-basin.

4 IMPLICATIONS FOR THE VOLCANOTECTONIC EVOLUTION OF THE ASAL–GHOUBBET RIFT

4.1 Seismogenic normal faulting

The Asal–Ghoubbet rift was the site of a strong earthquake sequence in November 1978, the main shocks of which occurred on November 7 and 8 ($m = 5.3$ and 5, respectively) in the Ghoubbet basin (Fig. 13). The sequence gave birth to a new volcano (Ardoukoba) that poured basalt flows at the northwestern tip of the Asal rift from November 7–14 (e.g. Abdallah *et al.* 1979). Many of the normal faults on land were

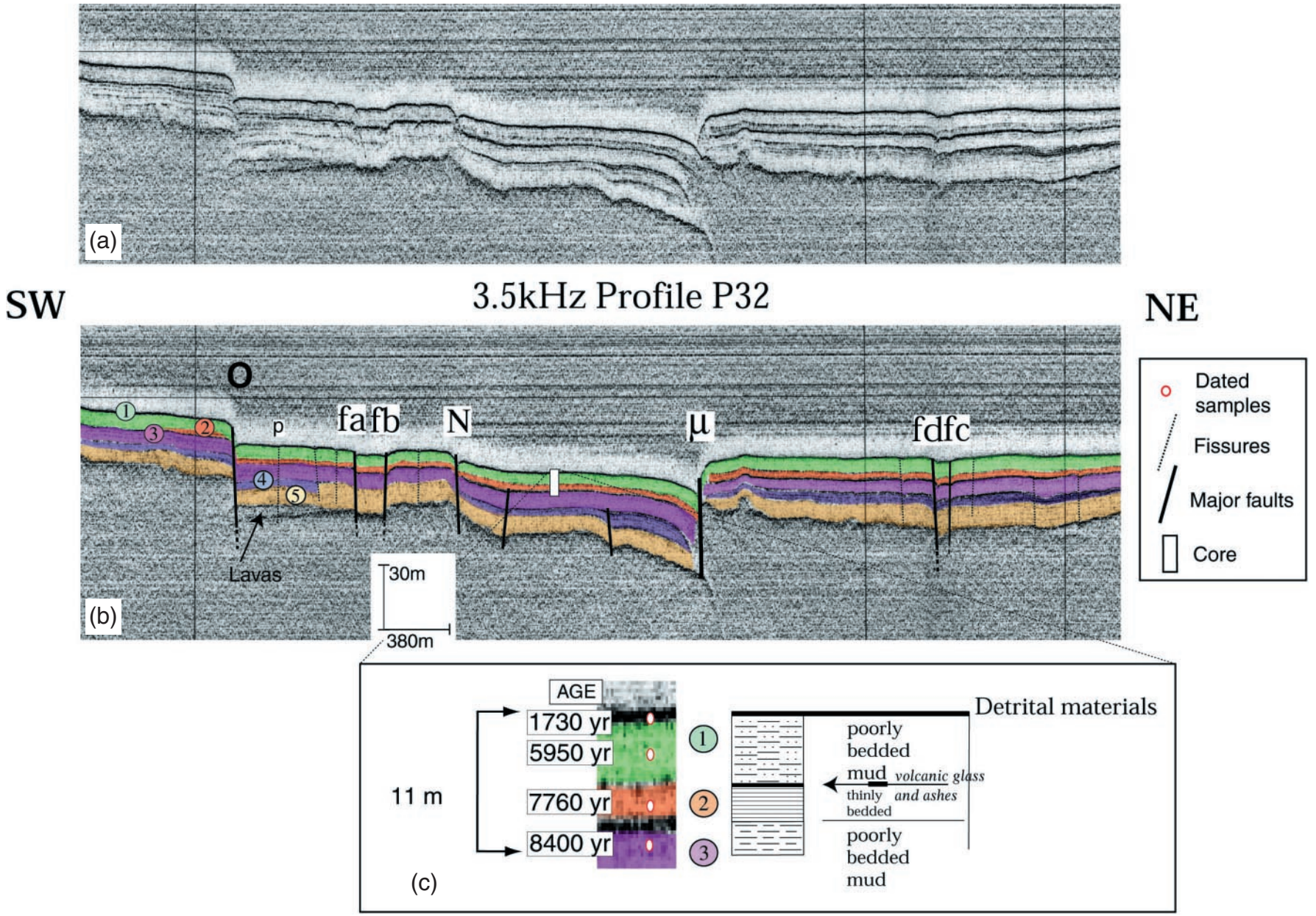

Figure 11. (a) 3.5 kHz profile P32 (see location in Fig. 2a). Colours represent individual sediment layers on the southern side of Ghoubbet volcano. Fault names and locations are from Fig. 6. Fault locations are coherent with fault traces identified in the bathymetric map of Fig. 2. (b) Projection of core A and interpretation of faulted sedimentary cover along profile P32. Symbols and colours as in Fig. 10. Numbers refer to the five different sediment layers identified in the profile from the top (1) top the bottom (5). (c) Ages from core A and corresponding sedimentology from CEPM–CNEXO (1981).

Table 1. Comparison, in northern (NB) and southern (SB) sub-basins, of average thickness of individual sediment layers as a function of total sediment thickness (from profile P8; Fig. 10). Reported depths with ages are from samples in core A near profile P32 (Fig. 11). The bottom layer appears to be made of basaltic flows. Apparent thicknesses are indicated only where both upper and lower interfaces have been identified.

	Layer 1	Layer 2	Layer 3	Layer 4	Layer 5	Volcanic layer
Individual thickness/ total thickness (m) (SB, P8)	5.5/5.5	4/9.5	9.5/19	9.5/28.5	11.5/40	9.5/49.5
Sample depth (m)/ Age (a from P32)	0.5–3.5/ 1730 ± 210/ 5950 ± 300	8.5/ 7760 ± 370	11/ 8400 ± 300	–	–	–
Individual thickness/ total thickness (m) (NB, P8)	9.5/9.5	9.5/19	11.5/30.5	–	–	16/46.5

reactivated, and numerous new surface breaks or open fissures were mapped (e.g. Abdallah *et al*. 1979; Le Dain *et al*. 1979; Jacques *et al*. 1996; Stein *et al*. 1991; Manighetti *et al*. 1998). At the time, no evidence of submarine faulting could be observed in the Ghoubbet. Superimposing the location of the shocks and aftershocks that occurred from November 7 to December 21 on our structural map shows that both the main shocks and the most immediate aftershocks (from November 10–12) are principally located within the axial graben, between faults O and μ. The November 7 main shock occurred beneath the northwestern tip of the axial graben inner floor, while most of the other important shocks occurred in or near the south-eastern sub-basin. The latest aftershocks, also mostly in the southeast (from November 12 to December 21), tend to be more spread out, as expected from modelling local Coulomb stress variations (e.g. Lépine & Hirn 1992; King *et al*. 1994; Jacques *et al*. 1996). The focal mechanisms calculated for the two main shocks are consistent with dominant left slip on N150–160°E-striking planes. Such dominant sinistral slip is unexpected in the axial graben of the rift, although it is compatible with the sinistral component of slip inferred from geometry on the N120–130°E normal faults (e.g. Manighetti *et al*. 1998). The process, however, is similar to what was observed for the 1960 Serdo sequence (e.g. Tapponnier *et al*. 1990; Jacques *et al*. 1996). The sinistral components probably result from clockwise block rotation (Manighetti 1993). In any case, the coincidence between the 1978 main event epicentral locations and the fault traces confirms that the main Ghoubbet faults are presently active, in keeping with the fact that they offset sediments deposited in the last few thousand years and are marked by sharp scarps on the sea bed.

4.2 Cumulative vertical offset measurements

On most of the 3.5 kHz profiles, the layers within the sediment cover of the Ghoubbet floor are particularly easy to separate from one another because their top surfaces show up as dark lines (indurated beds due to more detrital elements, or perhaps even, for a few of them, due to drying, Fig. 14a and b). On profiles crossing fault scarps nearly perpendicularly (P33 and P32 on Fig. 2a), it is thus possible to measure the vertical offsets of the successive layer top surfaces across the faults. Maximum offsets are generally measured for the volcanic basement surface beneath the sediment cover (Fig. 14b). Minimum offsets are obtained for the seafloor (water–sediment interface at the top surface of layer 1, Fig. 14b). We considered only offsets greater than 0.5 m (half of the estimated 1 m relative accuracy).

There may be subtleties involved in measuring the offsets of the sedimentary interfaces visible on the 3.5 kHz profiles (Figs 5, 9 and 11). The reference surfaces whose offset is measured across each fault are parallel to bedding in the successive layers on the footwall and hanging wall. In general, such surfaces are nearly horizontal. The offset is measured vertically, roughly perpendicular to these surfaces, midway between the piercing points (Fig. 14b). Given the very steep dip of the faults, this provides a good measure of the offsets. In the simplest cases, one can define undisturbed horizontal surfaces on either side of an isolated fault (e.g. Fig. 11, fault O). In more complicated cases, extrapolation of one, or two, of the reference surfaces across ambiguous zones with localized flexure or cracking may be needed. Such cases are illustrated by examples in the southwest part of profile P33 (Fig. 9, fault ω; Table 2); fault μ on P32 (Fig. 11, Table 3). In some other cases, the reference surfaces are hard to define because of the short spacing of the faults (Fig. 9) and/or vertically varying dips, which results in perturbed, short and curved horizons. Examples of this sort exist in the central part of profile P33 (e.g. Fig. 9, between faults f6 and f9; Table 2). For faults f2, N and M, the reference surface used to estimate the offset is

Table 2. Vertical offsets of layer top surfaces (S1 = top surface of layer 1, etc.) by faults on profile P33 (NW sub-basin); asterisks indicate faults common to both P32 and P33.

	P33	Offset S1 (m)	Offset S2 (m)	Offset S3 (m)	Offset S4 (m)
*	O	10.3	10.3	10.3	–
	f8	2.8	2.8	2.8	–
	f2	1.9	1.9	1.9	–
*	N	12.2	14.5	16.9	–
	f6	3.8	5.2	6.6	–
*	M	6.6	6.6		–
	f7	3.3	3.3	4.7	10.8
	f9	2.3	2.8	3.8	8.4
*	μ	9.3	11.7	17.8	17.8
	f10	0.9	1.9	1.9	–
	ω	3.8	3.8	5.6	–

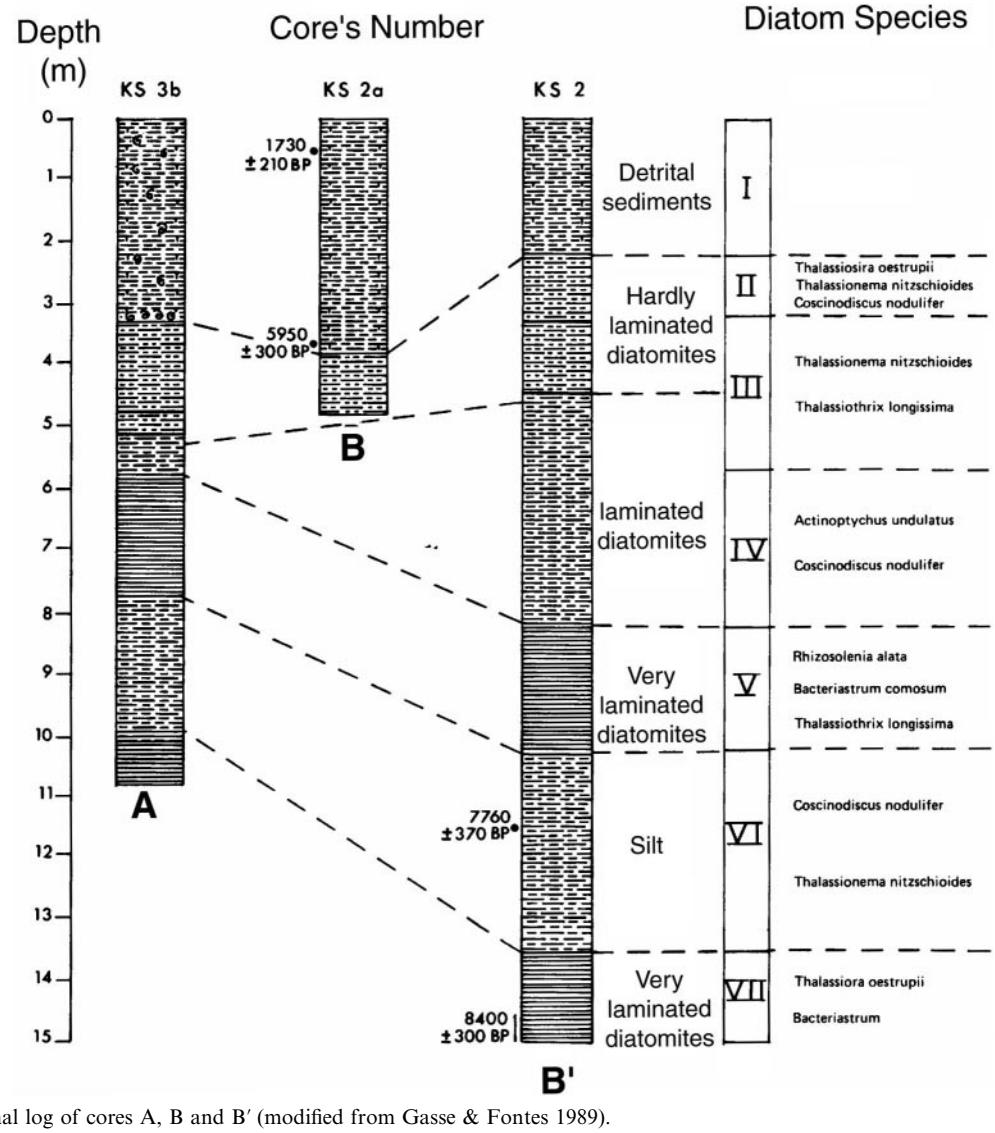

Figure 12. Original log of cores A, B and B′ (modified from Gasse & Fontes 1989).

approximated by a horizontal tangent to the top of the sediment interface. The offset may in this case be slightly overestimated (Table 2).

A test for self-consistency is to compare the offsets, by the same fault, of successively deeper sediment interfaces, since a shallow interface cannot be offset more than a deep one. The measured vertical offsets (P3, Fig. 5; P33, Fig. 9; P32, Fig. 11) of each layer interface identified in the two sub-basins are reported in Tables 2, 3 and 4. The fault throws range from ~1 to ~40 m. The lower volcanic basement usually shows much larger amounts of throw than recorded by the sediment–water interface (Fig. 14b). In addition, offsets of the same interfaces by faults common to two profiles are often of the same order (Tables 2 and 3).

Since certain interfaces with different ages and depths show different offsets, we plotted such offsets as a function of depth (Fig. 15). On such plots, it is possible to distinguish synsedimentary slip from post-depositional cumulative slip

Table 3. Vertical offsets of layer top surfaces by faults on profile P32 (southern sub-basin); asterisks indicate faults common to both P32 and P33 (Figs 9 and 11).

	P32	Offset S1(m)	Offset S2(m)	Offset S3(m)	Offset S4(m)	Offset S5(m)	Offset S6(m)
*	O	11.2	11.2	11.2	14.1	16	20.7
	fa	2.8	2.8	2.8	2.8	–	5.2
	fb	2.3	2.3	2.3	2.3	–	2.3
*	N	9.8	9.8	10.8	12.3	–	14.1
	fc	2.3	2.8	2.8	2.8	2.8	–
	fd	2.3	2.3	2.3	2.8	5.2	–
*	μ	10.3	10.3	10.3	15.1	?	28.9

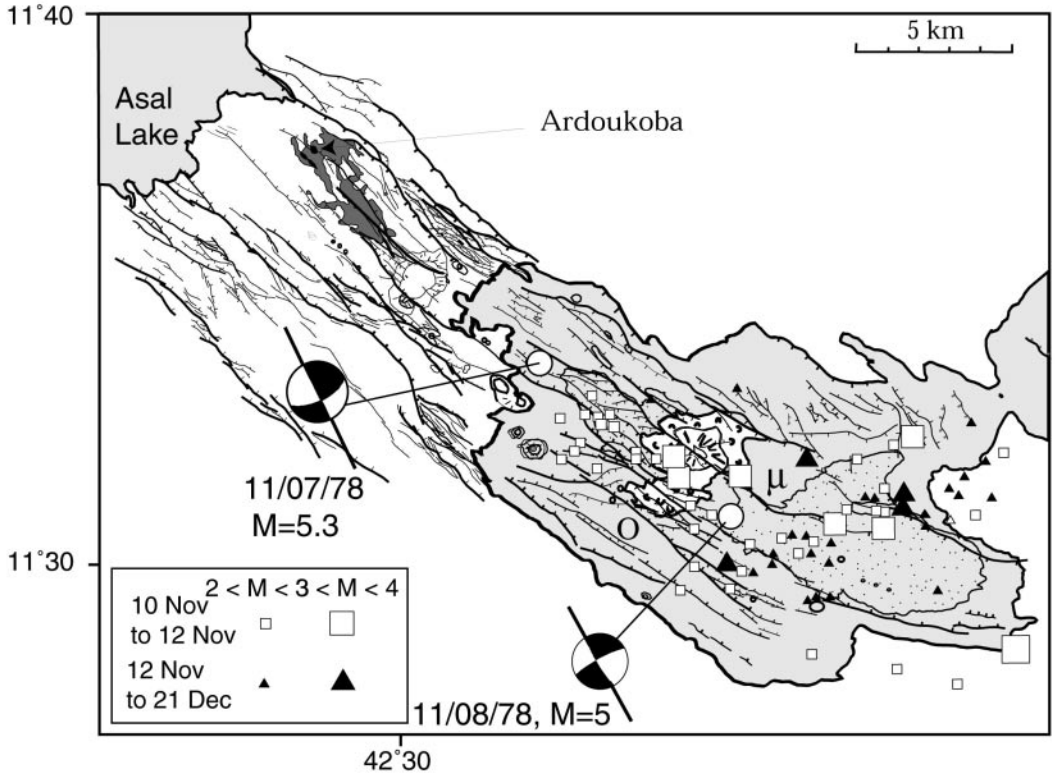

Figure 13. Seismotectonic map showing the locations of the main shocks of the 1978 seismic sequence (Lépine & Hirn 1992) superimposed on the main faults from the tectonic map of Fig. 6.

(Fig. 15). On most faults, it is clear that the successive layers recorded both post- and synsedimentary slip. The cores yield age control on the upper sediment layers (green, orange and violet in profile P32, Fig. 11) in the SW sub-basin. The lower part of the top (green) layer is 5950 yr old. The base of the second layer (orange, Fig. 11) is about 7760 yr old, and the top of the third about 8400 yr old (violet, Fig. 11). Given such ages, offsets may then be used to estimate vertical throw rates on the faults. In general, three rates may be calculated. They are discussed below.

4.3 Vertical slip rates

A particularly good example of interaction between sedimentation and faulting is that of fault O (profile P32, Fig. 15a). Both the offsets and the ages of positioned ^{14}C-dated samples are plotted as a function of depth to the top of the layer interfaces on the hangingwall. The consecutive layers show either constant or growing offset with depth. The shallowest interfaces, S1, S2 and S3, have the same offset (11.2 m), whereas the deeper ones (S4, S5, S6) display an increase to 14.1 m, then 16 m and finally 20.7 m. Such offsets place bounds on the vertical throw rate, given the ages of the layers (Fig. 15a). If one assumes, for instance, the 11.2 ± 1 m offset of S1, S2 and S3 to be younger than 5950 ± 370 a (upper ^{14}C age in green layer, Fig. 11), a maximum vertical slip rate of 1.9 ± 0.3 mm yr^{-1} ensues, smaller than the maximum rate proposed by Stein *et al.* (1991) on the same fault of ~ 4 mm yr^{-1}. Taking the older age (7760 ± 370 a) of the second layer would yield a slower throw rate of 1.45 ± 0.3 mm yr^{-1} (Table 5). With the age of 8400 ± 300 a of layer 3, one obtains a vertical slip rate of 1.35 ± 0.3 mm yr^{-1}, which might be taken to be representative of the average rate during much of the Holocene (Table 5).

Table 4. Vertical offsets of layer top surfaces by faults on profile P3 (northern sub-basin); asterisks indicate faults common to P32, P3 and P33 (Figs 5 and 9,11).

	P3	Offset S1 (m)	Offset S2 (m)	Offset S3 (m)	Volc1 (m)	Volc2 (m)
*	f7	3.8	3.8	–	3.8	5.7
*	f6	4.75	5.7	–	9.5	–
*	N	8.5	10.5	–	11.5	–
	P	14.25	–	–	19	–
*	f9	1	1	1.9	–	–
*	M	4.75	6.7	–	8.6	–
*	O	17.1	17.1	–	17.1	–
*	μ	23.5	–	–	39.2	–
*	ω	27.5	27.5	27.5	31.4	39.2

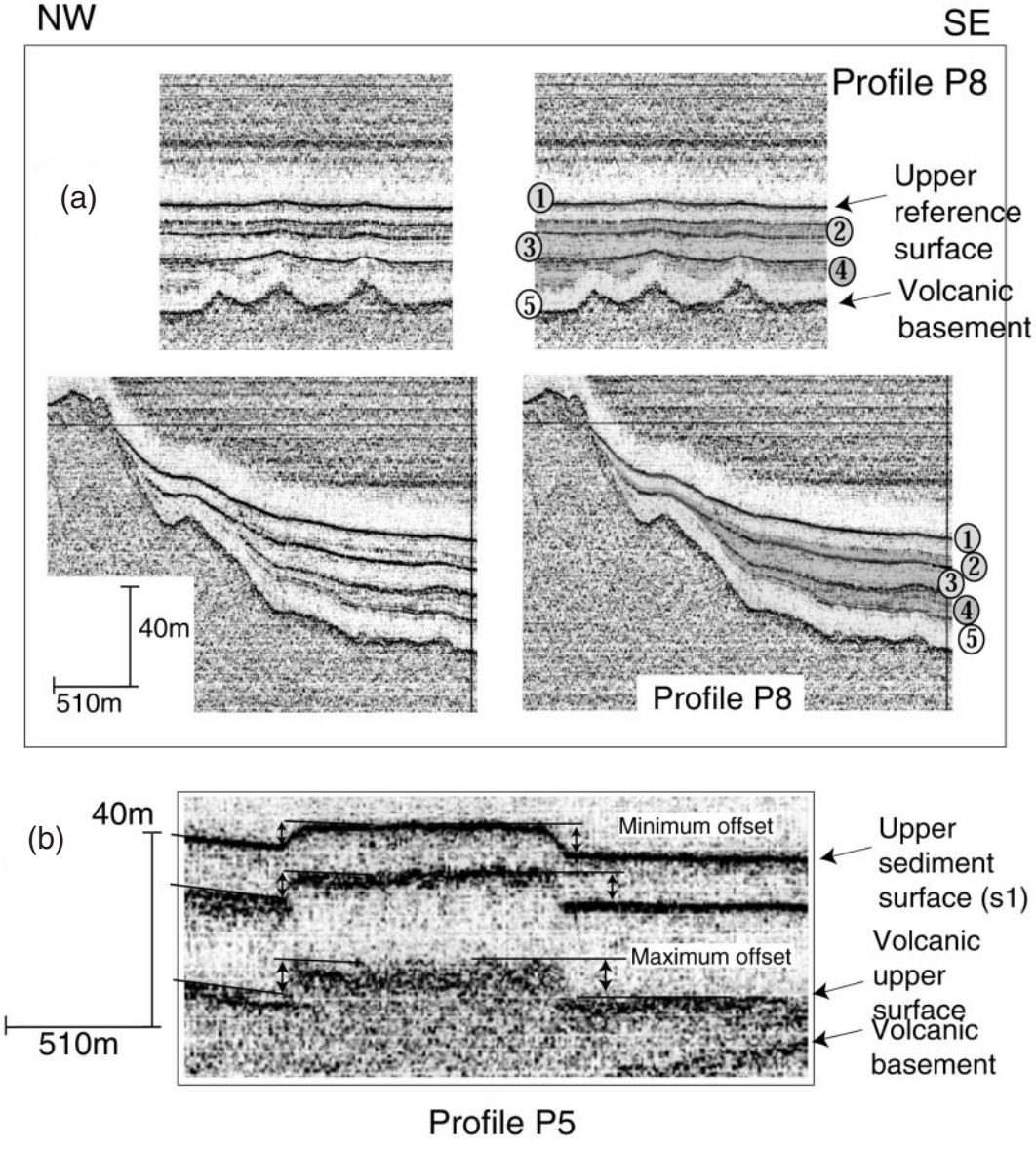

Figure 14. (a) Enlargements of sections of profile P8 showing changes in thickness (assuming a 1500 m s^{-1} velocity) and pinching out of layers 3 and 4. Numbers refer to the five different sediment layers identified and labelled on profile P32 (Fig. 11). (b) Example of offset measurements of layer interfaces on 3.5 kHz profile P5.

Table 5. Comparison of vertical slip rates, calculated on faults identified on P32, where core samples are dated. Maximum vertical rates are calculated using offsets recorded by layer 1 with an age of 5950 ± 300 yr. Mean Holocene throw rate is calculated from offset of layer 3 with an age of 8400 ± 300 yr (Fig. 11).

	P32	Max. vertical rate (mm yr^{-1})	Rate for offset of 2d layer (mm yr^{-1})	Mean Holocene vertical rate (mm yr^{-1})	Stein *et al.* (1991) Hol. vert. rate (mm yr^{-1})	De Chabalier (1993) Hol. vert. rate (mm yr^{-1})
*	O	1.9	1.45	1.35	(E) 0.8	2.3
	Fa	0.45	0.35	0.33	–	–
	Fb	0.4	0.3	0.3	–	–
*	N	1.65	1.25	1.3	(D) 1.4	–
	Fc	0.4	0.45	0.45	–	–
	Fd	0.4	0.4	0.4	–	–
*	μ	1.75	1.3	1.25	(γ) 1.3	(γ, α) 1.4

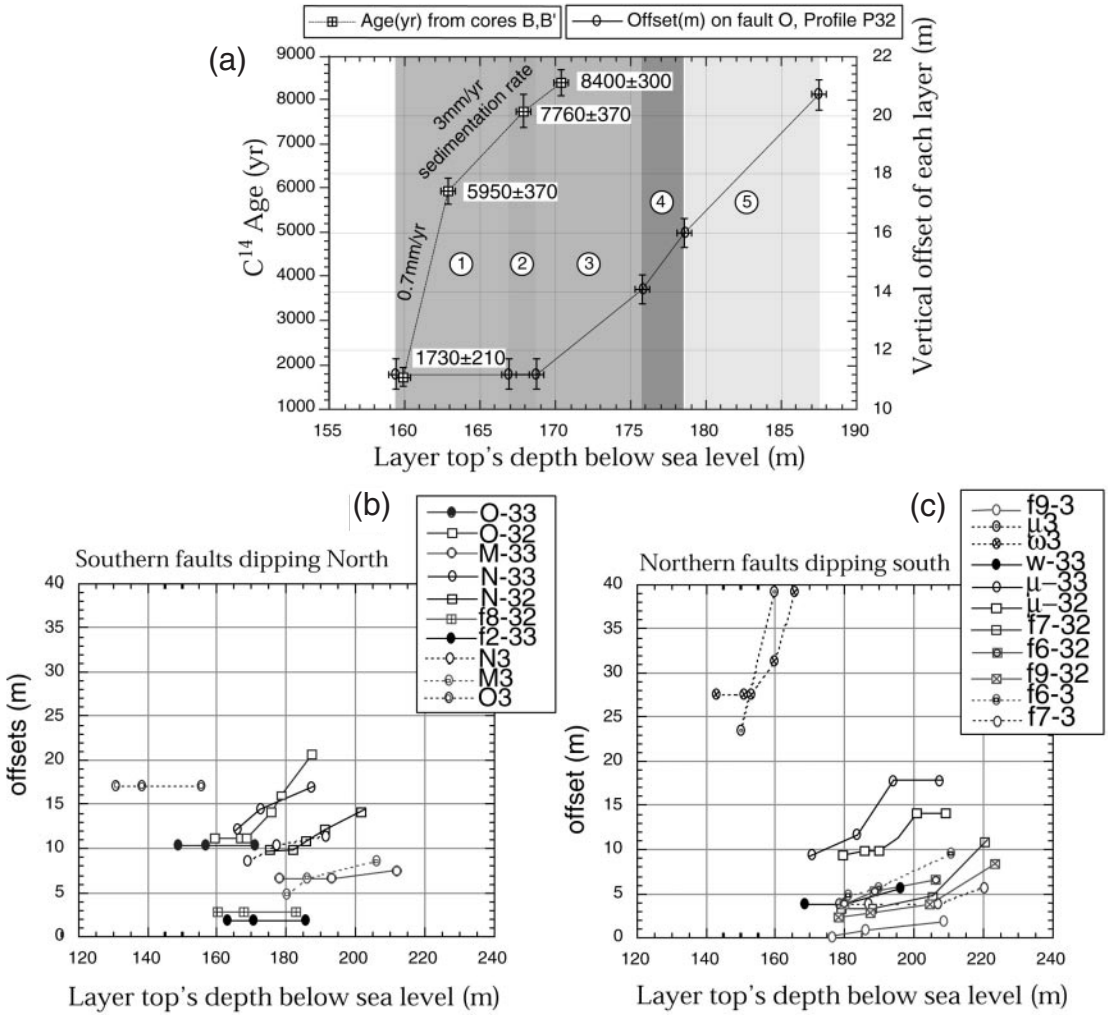

Figure 15. (a) Plot of vertical offsets on fault O as deduced from individual sediment layer thicknesses and depths of dated samples. Circles correspond to vertical offsets measured on each sediment layer surface identified in Fig. 9(a). Squares indicate ^{14}C ages as a function of depth for each dated sample from cores B and B′. (b) and (c) Vertical offsets across Ghoubbet submarine faults. The shapes of the symbols correspond to different offsets on the same fault. Offsets are for top surfaces of either sediment or volcanic layers identified on 3.5 kHz profiles P3, P32 and P33. Faults may be represented several times because they are crossed by several profiles (e.g. μ). Southern faults dipping north and northern faults dipping south have been separated.

The offsets of the base of the upper layer, where identified, always provide upper bounds on the vertical throw rates on each fault (Table 5). Such maximum throw rates range between 0.4 ± 0.3 and 1.9 ± 0.3 mm yr^{-1}. The offsets of the third layer, the deepest one dated (8400 ± 300 a) provide mean Holocene vertical slip rates ranging from 0.3 ± 0.3 to 1.35 ± 0.3 mm yr^{-1} (Table 5). Such rates are similar to those calculated by Stein *et al.* (1991) and Manighetti *et al.* (1998) for the main faults of the Asal rift.

4.4 Subrift organization

Vertical offsets on the faults do not appear to increase as a function of distance from the rift axis (Fig. 16a), but the cumulative vertical offset does (Fig. 16b). Extensional strain is thus not just localized at the axis but is spread over much of the central part of the rift (Fig. 16a). The plot of vertical offset versus distance from the rift axis is consistent with the existence of three subrifts, visible in map view, which are limited by the three major faults O, N and μ (Fig. 17). These boundary faults seem in fact to be as active as possibly younger ones near the rift axis (Fig. 16a). The major faults (O, N, μ and ω) bound the deepest troughs on the Ghoubbet floor. Inside each trough, smaller antithetic faults meet these main faults to define wedge-shaped tips that point towards the west (Fig. 17). This organization in narrow elongated subrifts that taper westwards is analogous to that identified on land and thus likewise suggests propagation of rifting towards the NW. The submarine subrift tips resemble in fact that of Dankalelo (Fig. 2), where many small antithetic faults meet a main normal fault (Manighetti *et al.* 1998). This geometry appears to typify most submarine fault connections within each *en echelon* subrift (SR1, SR2 and SR3 from SW to NE on the Ghoubbet floor; Fig. 17). It is therefore possible to extend and generalize for the entire Asal–Ghoubbet rift the model of subrift organization

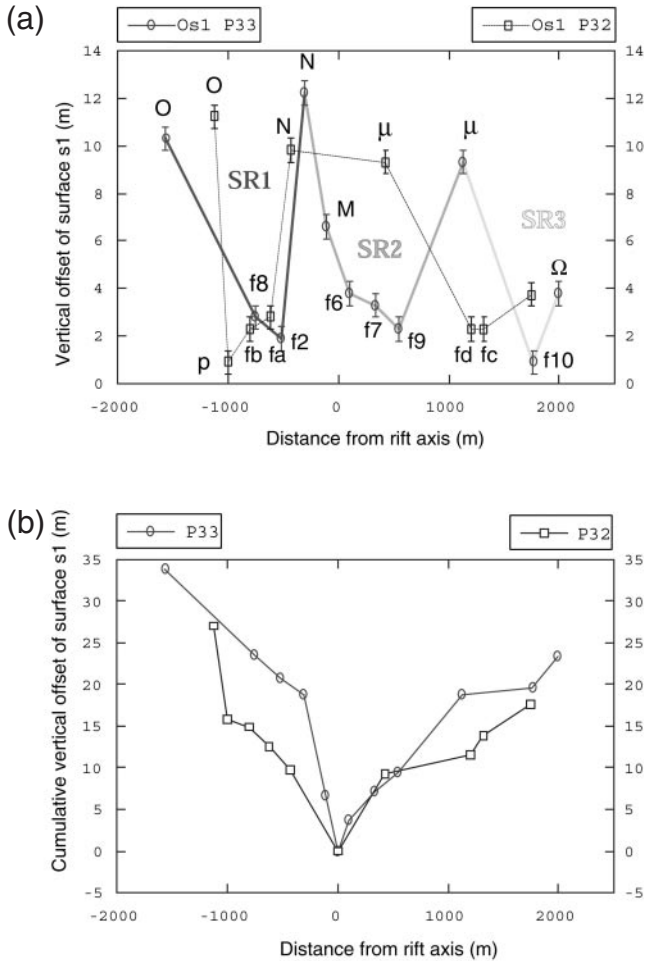

Figure 16. (a) Vertical offset of top surface S1 (Os1) for each fault identified on P32 and P33 as a function of distance from the rift axis. SR1-3 refers to subrifts identified in map view. (b) Cumulative vertical offset of faults as a function of distance from the rift axis

defined on land by Manighetti *et al.* (1998). This model included only two subrifts and a migration of the most recent deformation towards the northern subrift (Disa Le Mallo, SR3, DiS, Fig. 17), which seemed more seismically active than the southern Dankalelo (DaS and SR1) subrift. The overall generalized model (Fig. 17) based on the new bathymetric data involves three narrow *en echelon* subrifts, all with tips directed northwestwards, and supports the idea of propagation of volcanism and rifting in that direction. The northernmost two of the three partly emerged subrifts (SR2 and SR3) were activated by the 1978 seismic sequence. They show segmentation in map view (Figs 2 and 13), as confirmed by the different vertical throws of the corresponding antithetic fault system (Figs 13, 15 and 16). The SW subrift geometry appears to be different from that of the NE subrifts. SR1 is narrower and mostly limited by faults dipping towards the NE, whereas SR2 and SR3 are broader and bounded by antithetic faults with greater throws. The Asal–Ghoubbet rift is thus a composite feature, formed by three parallel subrifts that terminate northwestwards with narrow tips. The biggest central volcanoes (Fieale and Ghoubbet volcanoes), however, are located along or at the edge of the central subrift (SR2).

5 PALAEOENVIRONMENTS AND SEDIMENTATION IN THE GHOUBBET

5.1 Asal and Ghoubbet hydrology

Holocene water level fluctuations in Lake Asal (Figs 2 and 13) have been reconstructed by Gasse & Fontes (1989). The present-day hypersaline lake lies within a narrow and deep basin, limited by NW–SE-trending fault scarps, with cumulative throws of up to 1000 m (Fig. 2). The topographical and hydrological situation of the lake, 155 m below sea level and only 15 km from the open sea, is thus exceptional (Fig. 18a). However, the low-stand of the lake is rather recent. After the arid phase at the end of the Pleistocene, the Holocene period began with a high Asal lake level (at 310 m elevation above present lake level) from $\sim$8.6 to $\sim$6 ka. During this Early Holocene climatic optimum highstand, Lake Asal received a large part of the water excess flowing from the Ethiopian highlands, mostly through underground water supply from Lake Abhe (Gasse & Fontes 1989). The Ghoubbet was then the terminus, leading into the open sea through the Ghoubbet Strait, of a system of lakes cascading into one another (Fig. 18b). The Fieale volcano divided the Asal rift into secondary basins and favoured the development of separate bodies of water (Lake Asal and Ghoubbet) (Fig. 2). The drainage of the Ethiopian hydrological system into the Ghoubbet was effective at least until about 9000 yr ago, when the sea returned to roughly its present-day level. Subsequently, a rapid and dramatic regression of the Asal lake level (down to $\sim$150 m below present sea level) occurred from 6 to 5 ka as continental water input dwindled and was replaced by marine infiltration from the Ghoubbet. Today, the major water input to the lake is this infiltration of Ghoubbet water through the tectonic fissures of the Asal rift (Fig. 18a). Such reversal of water inflow probably also occurred during past dry periods.

A drastic change in sedimentation, synchronous with the regression at Asal, is observed in the Ghoubbet basin. The early Holocene deposits are mostly pure laminated diatomites with typical marine planktonic flora, whereas fine detrital material appears to predominate after 5.95 ka (Gasse & Richard 1981; Gasse & Fontes 1989; Fig. 12). Also, between about 9 and 6 ka, the sedimentation rate in the Ghoubbet was about 3 mm yr^{-1}, about four times that observed since then (0.7 mm yr^{-1}, Fig. 15). Because the total thickness of the sediments deposited on the volcanic floor of the Ghoubbet is <60 m, such sediments are probably not well compacted and still full of water. They probably form a mud, denser than water, thus able to flow into the deepest areas. This may explain the variations in thickness and distribution of layers 3 and 4 inside the Ghoubbet basin (P32, Figs 11 and 14a). Such flowing mud may have reworked non-marine deposits, leading to heavy suspension loads and relative turbidity, resulting in the filling of the deepest fault troughs and fissures and the masking of some tectonic activity.

5.2 Shallow entrance of the Ghoubbet 'lake' and fluctuation of sea level

Profile P3 (Location in Fig. 2), from the Tadjoura Gulf to the Ghoubbet SW coast, images all structures across the shallow Ghoubbet Strait (Fig. 19). To the east, a rather smooth seafloor appears to deepen gently into the Gulf of Tadjoura. The Ghoubbet Strait is floored by a rugged volcanic surface cut by

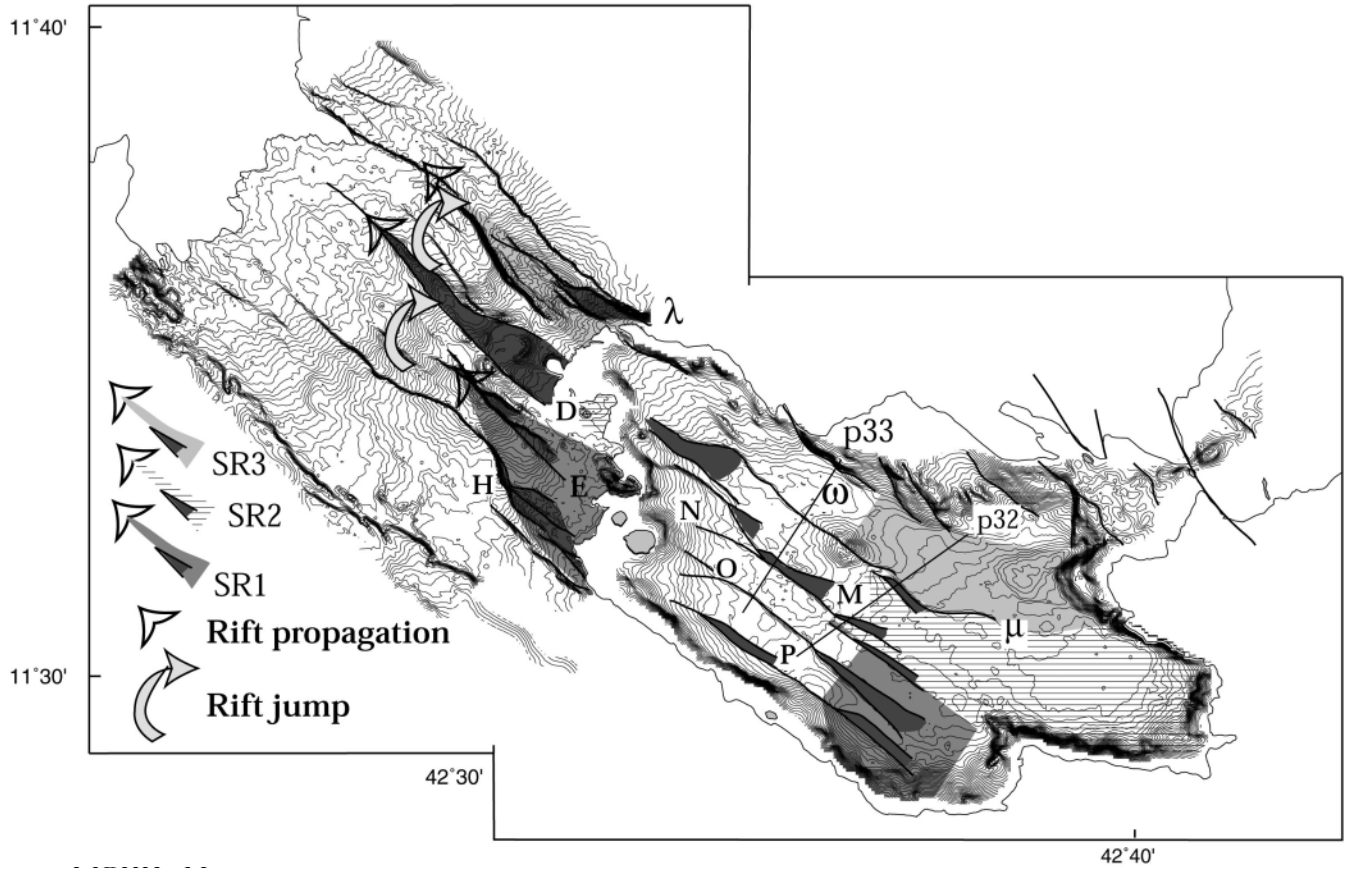

Figure 17. Subrift organization in map view and propagation interpretation along the Asal–Ghoubbet rift. Faults in black bound sub-basins whose floors taper towards the NW, themselves nested inside the three main subrifts. DiS: Disa Le Mallo subrift; DaS: Dankalelo subrift.

normal faults (Fig. 19a). At 42°39′E, in particular, a steep N–S-striking, W-dipping normal fault (Fig. 19a), with a vertical throw of about 100 m, oblique to the main Ghoubbet faults, bounds the deepest area of the Ghoubbet basin. The depth of the strait is everywhere less than 100 m and the minimum depth only about 23 m. The thin (less than a few metres thick) layer of sediments that partly covers the volcanic basement on either side of the strait is interrupted across the shallowest part.

Quantitative knowledge of recent global fluctuations of sea level (<140 kyr, Chappell *et al.* 1996) implies that the sea-level drop that exceeded 120 m about 18 000 yr ago should have isolated the Ghoubbet from marine influence (Figs 18c and 19c) with complete emergence of the strait over a width of several kilometres. As this occurred, the water level of the Ghoubbet lake probably dropped because of the dry climate. Consequently, the Ghoubbet volcano could have divided the Ghoubbet into two basins as Fieale now separates lake Asal from the Ghoubbet (Fig. 18c). A different regime would thus have governed the deposition of sediments in the northwestern (P33, Fig. 9) and southeastern sub-basins (P32). Based on the mean Holocene throw rates calculated on the submarine faults of the Ghoubbet, it is possible to estimate the age of the deepest reflective interfaces (sediments or volcanic flows) given their offsets. The total vertical offset of the volcanic basement sediment interface identified on P32 (beneath the yellow sediments in Fig. 11) being about 29 m across fault μ (Table 6), the mean vertical slip rate on this fault (1.25 ± 0.3 mm yr^{-1}) would yield a minimum age of ~23 000 yr for this volcanic surface and of ~12 000 yr for the fourth layer top surface. With Fault O, an age of 15 300 yr is obtained for the basement.

Such ages suggest that layers 4 and 5, and possibly the bottom part of layer 3, which is older than 8400 kyr, may have been deposited in a continental lake environment, during a dry period in which the Ghoubbet was isolated from the global

Table 6. Maximum vertical offsets of layer S6 by major faults on profile P32 (SE sub-basin) and the calculated age of the volcanic floor of the SE Ghoubbet sub-basin.

	Mean Holocene vert. rate (mm yr^{-1})	Offset of S4 (m)	Offset of S6 (m)	Age of S4 (=sediment surface)	Age of S6 (=volcanic surface)
fault O	1.35	14.1	20.7	~10 500 yr	~15 300 yr
fault μ	1.25	15.1	28.9	~12 000 yr	~23 100 yr

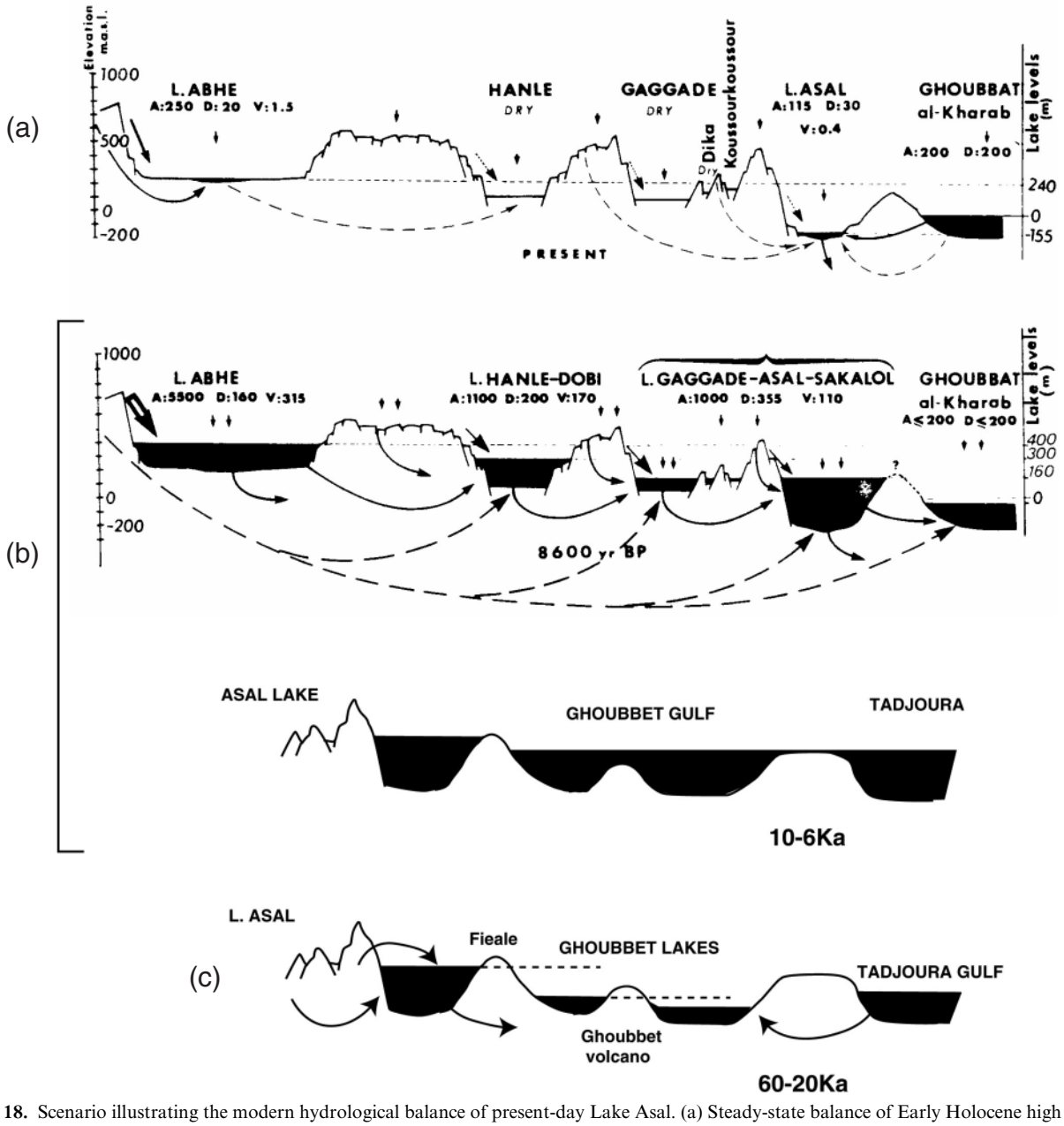

Figure 18. Scenario illustrating the modern hydrological balance of present-day Lake Asal. (a) Steady-state balance of Early Holocene high level at 8600 yr BP; (b) after Gasse & Fontes 1989; (c) inferred glacial age situation.

ocean (Fig. 19c). A low level of the lakes, due to evaporation, as observed today at Asal, would explain the different numbers and thicknesses of layers in the eastern and western sub-basins on either side of the Ghoubbet volcano and might explain the heterogeneity of layer 4's thickness along profile P32 (e.g. between μ and N in Fig. 11).

If we consider that the faults north of the Ghoubbet Strait chiefly accommodate sinistral motion due to bookshelf faulting (Manighetti 1993), their throw rate should be a fraction of their horizontal rate, and smaller than the throw rates of the rift normal faults, i.e. probably less than 1 mm yr^{-1} (Fig. 6). Given the present average minimum depth of $\sim$30 m of the Ghoubbet Strait horst, vertical uplift at rates of the order of 0.5 mm yr^{-1} would imply that the Ghoubbet was cut off from the sea prior to 10 kyr BP (Fig. 19c). Assuming a continuous throw rate of 0.5 mm yr^{-1} on the faults bounding the Ghoubbet Strait horst, it would have stood only 50 m below the present sea level when the Ghoubbet basin became isolated from the sea about 72 000 yr ago. Taking the present evaporation rate in the region (2.65×10^6 m^3 yr^{-1}, Dosseur 1977) to be representative of that 72 000 yr ago, it would have taken only about 4000 yr to dry the entire basin if it contained an overall water volume of about $100 \times 7300 \times 14600 = 106 \times 10^8$ m^3 (Fig. 19c). Large areas of the Ghoubbet basin were thus probably reduced to disconnected brine pans during much of the last Glacial age (70–10 kyr BP), even if one takes into account tectonic uplift rates of the Ghoubbet Strait horst of the order of 0.5 mm yr^{-1}, almost certainly a maximum. The lowermost layers of sediments in the southern basin, closest to the strait (fourth violet and fifth yellow layers), are thus probably composed of nearly

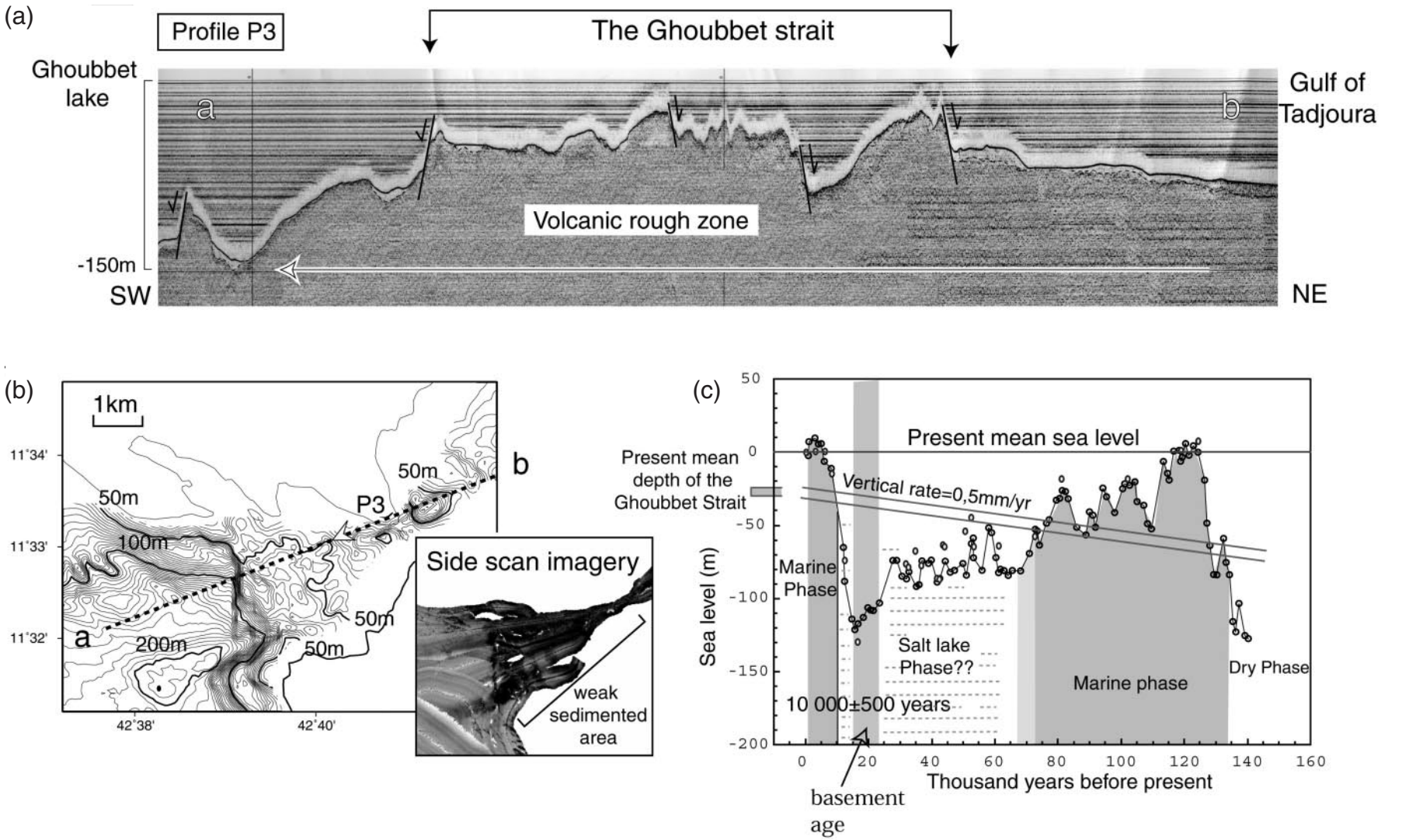

Figure 19. (a) 3.5 kHz profile P3 (see location in Fig. 2a) across the volcanic horst bounded by normal faults corresponding to the Ghoubbet Strait between the Gulf of Tadjoura and Ghoubbet Al Kharab. (b) Precise bathymetry of the Ghoubbet Strait and side-scan imagery from Fig. 4(a). Dark zones are volcanic surfaces or surfaces free of sediments due to temporary immersion or sea-bottom currents. Grey areas are sedimented. (c) Relationship between sea-level fluctuations deduced from coral terrace elevations at Huon Peninsula and deep sea core O^{18} data from Chappell *et al.* (1996) and marine flooding of the Ghoubbet Gulf as a function of tectonic uplift rate of the Ghoubbet Strait horst.

pure evaporites (mostly halite). This might explain why these bottom layers tend to smooth the relief of the volcanic basement, whether it be due to faulting (Fig. 11) or to lava effusion (Fig. 14a).

6 SUMMARY AND CONCLUSIONS

The 1995 Tadjouraden survey of the Ghoubbet sea gulf provides a much improved view of recent volcanism and tectonic faulting along the Asal–Ghoubbet trough, the westernmost rift segment of the Aden propagator. By combining the new geophysical evidence obtained at sea with the detailed results of many previous studies on land we propose an integrated model of the evolution of this rift.

Much of the Ghoubbet basin displays a rift-in-rift structure, roughly aligned with that of the emerged Asal rift ($\sim$N130°E). The maximum depth (about 220 m) is attained in a small NE-striking transverse trough just south of the Ghoubbet. The 3.5 kHz mud penetrator profiles show that the Ghoubbet floor is covered by a $\sim$50 m thick sediment blanket composed of several well-defined layers with strongly reflective upper interfaces. Most of the sediments appear to have been deposited on a $\sim$15–23 000 yr old volcanic basement.

The sediments and basement are cut by normal faults, whose antithetic pairing helps define three subrifts that taper westwards, a geometry that we interpret to reflect propagation in this direction, as inferred at Asal (Manighetti *et al.* 1998). Calibration of the ages of the sedimentary column with ^{14}C-dated cores (CEPM–CNEXO 1981) yields throw rates on the faults of 0.3–1.4 mm yr^{-1}, similar to those found on land by Stein *et al.* (1991), De Chabalier & Avouac (1994) and Manighetti *et al.* (1998). Like those along the emerged Asal rift, the submarine Ghoubbet faults exhibit a component of sinistral slip, reflected on the seafloor by the existence of small N80°E-striking fault scarps in left-stepping jogs of the main faults (e.g. fault μ) or by horsetail fault terminations. This is in keeping with sinistral slip on N150°E-striking planes, consistent with the focal mechanisms of the two main shocks of the 1978 seismic sequence (Ruegg *et al.* 1979), whose hypocentres were located under the Ghoubbet. Most of the large faults on land (e.g. α) have a submarine equivalent (e.g. ω), which implies rough continuity of such features through the crust.

A submarine central volcano, the Ghoubbet volcano, sits in the middle of the Ghoubbet floor, dividing it into two distinct basins to the NW and SE. This volcano belongs to the volcanic axial line along which basaltic accretion takes place, and resembles the Fieale volcano, which separates Lake Asal from the Ghoubbet. Like the latter, it is cut by normal faults, but it is smaller and appears to be younger (20–30 kyr old versus 90–150 kyr old). That the Ghoubbet volcano is fairly young probably accounts for its roughly circular shape, which contrasts with the elliptical shape of Fieale, due to long-term finite extension at a rate of 20 mm yr^{-1} in the NE direction, perpendicular to the rift (De Chabalier & Avouac 1994).

The numbers and thicknesses of the sedimentary layers in the two basins on either side of the Ghoubbet volcano are different. Five layers are observed in the SE basin but only two or three thicker ones in the NW basin. In the SE basin, the first layers above the volcanic basement show drastic thickness changes, which tend to smooth relief, across faults or on top of small volcanic vents and pinch out at about 160 m depth on the volcano's flank. Also, in the same basin, a fourfold decrease in sedimentation rate, from $\sim$3 to $\sim$0.7 mm yr^{-1}, appears to have occurred rather rapidly around 6 kyr BP.

We interpret the variations in sediment thickness to reflect isolation from, then subsequent flooding by, the sea as result of global sea-level changes modulated by the shallow threshold of the Ghoubbet Strait, which is only 25 m deep in places. The gradual drop in sea level during the Wurm Glacial age must have completely severed connection between the Ghoubbet basin and the Gulf of Tadjoura at some time after 80 kyr BP. Subsequently, the Ghoubbet trough was probably occupied by a salty lake, fed by groundwater inflow through tectonic fissures, either from the sea or from Asal and other cascading lakes in Ethiopia (Gasse & Fontes 1989), a situation comparable to that now characterizing Lake Asal.

The past water level and salinity of the Ghoubbet were thus probably subject to strong changes, in tune with wetter or dryer climate spells. During especially dry periods in particular, the relief of the Ghoubbet volcano must have divided the Ghoubbet into two small, shallow and salty lakes, with distinct sedimentation regimes, as Fieale now separates lake Asal from the Ghoubbet. It is possible that the two layers that smooth basement relief on the Ghoubbet floor are in fact made of salt. Around 11 000–10 000 yr ago, as a result of the rapid postglacial rebound of sea level, the sea would have flooded the Ghoubbet basin anew, leading to 4000 yr of fast, uniform sedimentation on either side of the volcano, throughout the Early Holocene Climatic Optimum. Starting about 6000 yr ago with the onset of dryer conditions, a gentler sedimentation regime was established in the Ghoubbet in tune with the drop of water level in Lake Asal. Deeper and more extensive drilling in the Ghoubbet should help test such inferences.

REFERENCES

Abdallah, A. *et al.*, 1979. Afar seismicity and volcanism, *Nature,* **282,** 17–23.

Augustin, J.M., Le Suave, R., Lurton, X., Voisset, M., Dugelay, S. & Satra, C., 1996. Contribution of the multibeam acoustic imagery to the exploration of sea-bottom, *Mar. Geophys. Res.,* **18,** 459–486.

Bäcker, H., Clin., M. & Lange, K., 1973. Tectonics in the Gulf of Tadjura, *Mar. Geol.,* **15,** 309–327.

Barberi, F., Tazieff, H. & Varet, J., 1972. Volcanism in the Afar depression: its tectonics and magnetic significance, *Tectonophysics,* **15,** 19–30.

CEPM–CNEXO, 1981. *Orgon IV, Golfe d'Aden, Mer d'Oman,* Centre National de la Recherche Scientifique (CNRS), Paris.

Chappell, J., Omura, A., Esat, T., McCulloch, M., Pandolfi, J., Ota, Y. & Pillans, B., 1996. Reconciliation of late Quaternary sea levels derived from coral terraces at Huon Peninsula with deep sea oxygen isotope records, *Earth planet. Sci. Lett.,* **14,** 227–236.

Choukroune, P. *et al.*, 1986. Tectonics of the westernmost Gulf of Aden and the Gulf of Tadjoura from submersible observations, *Nature,* **319,** 396–399.

Choukroune, P., Francheteau, J., Auvray, B., Auzende, J.M., Brun, J.P., Sichler, B., Arthaud, F. & Lépine, J.C., 1988. Tectonics of an incipient oceanic rift (the western extension of the Aden rift within the Gulf of Tadjoura, Republic of Djibouti), *Mar. Geophys. Res.,* **9,** 147–163.

Cochran, J.R., 1981. The Gulf of Aden: structure and evolution of a young oceanic basin and continental margin, *J. geophys. Res.,* **86,** 263–288.

Courtillot, V., Achache, J., Landre, F., Bonhommet, N., Galibert, P.-Y., Montigny, R. & Féraud, G., 1984. Episodic spreading and rift propagation: new paleomagnetic and geochronologic data from the Afar passive margin, *J. geophys. Res.,* **89,** 3315–3333.

Courtillot, V., Galdéano, A. & Le Mouel, J.L., 1980. Propagation of an accreting plate boundery: a discussion of new aeromagnetic data in the Gulf of Tadjurah and southern Afar, *Earth planet. Sci. Lett.,* **47,** 144–160.

De Chabalier, J.B., 1993. Topographie et déformation tridimentionnelle du rift d'Asal (Djibouti), *Thesis,* Inst. Phys. du Globe de Paris.

De Chabalier, J.B. & Avouac, J.P., 1994. Kinematics of the Asal Rift (Djibouti) determined from the deformation of Fieale volcano, *Science,* **265,** 1677–1681.

Demange, J., Stieltjes, L. & Varet, J., 1980. L'éruption d'Asal de novembre 1978, *Bull. Soc. Geol. Fr.,* **22,** 837–843.

Dosseur, H., 1977. *L'évaporation au Lac Asal,* DAFECO, Div. Hydrol., Paris.

Gasse, F. & Fontes, J.C., 1989. Paleoenvironnements and paleohydrology of a tropical closed lake (Lake Asal, Djibouti) since 10000 yr B.P., *Palaeogeog. Palaeoclimat. Palaeoecol.,* **69,** 67–102.

Gasse, F. & Richard, M., 1981. Les diatomées de quelques sondages de la campagne Orgon IV, in *Orgon IV, Golfe d'Aden, Mer d'Oman,* pp. 309–330, CEPM–CNEXO, Paris.

Institut Géographique National (IGN), 1953. *Tadjoura Geological Map, scale 1/100 000,* IGN, Paris.

Jacques, E., King, G.C.P., Tapponnier, P., Ruegg, J.C. & Manighetti, I., 1996. Seismic activity triggered by stress changes after the 1978 events in the Asal Rift, Djibouti, *Geophys. Res. Lett.,* **88,** 2481–2484.

King, G.C.P., Stein, R.S. & Lin, J., 1994. Static stress changes and the triggering of earthquakes, *Bull. seism. Soc. Am.,* **84,** 935–953.

Le Dain, A.Y., Robineau, B. & Tapponnnier, P., 1979. Les effets tectoniques de l'événement sismique et volcanique de novembre 1978 dans le rift d'Asal-Ghoubbet, *Bull. Soc. Geol. Fr.,* **22,** 817–822.

Lépine, J.-C. & Hirn, A., 1992. Seismotectonics in the Republic of Djibouti, linking the Afar Depression and the Gulf of Aden, *Tectonophysics,* **209,** 65–86.

Manighetti, I., 1993. Dynamique des systèmes extensifs en Afar, *Thesis,* Paris 6.

Manighetti, I., Tapponnier, P., Courtillot, V., Gruszow, S. & Gillot, P.-Y., 1997. Propagation of rifting along the Arabia–Somalia plate boundary: the Gulfs of Aden and Tadjoura, *J. geophys. Res.,* **102,** 2681–2710.

Manighetti, I., Tapponnier, P., Gillot, P.-Y., Jacques, E., Courtillot, V., Armijo, R., Ruegg, J.C. & King, G., 1998. Propagation of rifting along the Arabia–Somalia plate boundary: into Afar, *J. geophys. Res.,* **103,** 4947–4974.

Ruegg, J.C., 1974. Structure profonde de la croûte terrestre au moyen de grands profils simiques, application à l'étude des zones de distension, *Thesis,* Paris.

Ruegg, J.C. & Kasser, M., 1987. Deformation across the Asal-Ghoubbet rift, Djibouti, uplift and crustal extension, 1979–1986, *Geophys. Res. Lett.,* **7,** 745–748.

Ruegg, J.C., Lépine, J.C., Tarantola, A. & Kasser, M., 1979. Geodetic measurements of rifting associated with a seismo-volcanic crisis in Afar, *Geophys. Res. Lett.,* **6,** 817–820.

Ruegg, J.-C., Lépine, J.-C. & Vincent, C., 1980. Sismicité et microsismicité de la dorsale de Tadjoura, tectonique et frontière de plaques, *Bull. Soc. Géol. Fr.,* **22,** 917–923.

Ruegg, J.C., Kasser, M. & Lépine, J.C., 1984. Strain accumulation across the Asal-Ghoubbet rift, Djibouti, East Africa, *J. geophys. Res.,* **89,** 6237–6246.

Ruegg, J.C., Gasse, F. & Briole, P., 1990. Mouvements du sol holocènes dans le rift d'Asal à Djibouti, *C. R. Acad. Sci. Paris,* **310**, Serie II, 1687–1694.

Stein, R.S., Briole, P., Ruegg, J.C., Tapponnier, P. & Gasse, F., 1991. Contemporary, Holocene, and Quaternary deformation of the Asal Rift, Djibouti: implications for the mechanics of slow spreading ridges, *J. geophys. Res.,* **96,** 21 789–21 806.

Stieltjes, L., 1973. Evolution tectonique récente du rift d'Asal, TFAI, *Rev. Geogr. Phys. Geol.,* **XV,** 425–436.

Stieltjes, L., 1980. *Geological Map of Asal Rift, Republic of Djibouti, scale 1/50000,* Centre National de la Recherche Scientifique, Paris.

Tapponnier, P. & Varet, J., 1974. La zone de Mak'arassou en Afar: un équivalent émergé des 'failles transformantes' océaniques, *C. R. Acad. Sci.,* Ser. D, **278,** 209–212.

Tapponnier, P., Armijo, R., Manighetti, I. & Courtillot, V., 1990. Bookshelf faulting and horizontal block rotations between overlapping rifts in southern Afar, *Geophys. Res. Lett.,* **45,** 435–444.

Tazieff, H., Varet, J., Barberi, F. & Glia, G., 1972. Tectonic significance of the Afar depression, *Nature,* **235,** 144–147.

Varet, J. & Gasse, F., 1978. *Geology of Central and southern Afar, scale 1:50000,* Centre National de la Recherche Scientifique, Paris.